

AD-A201 605

AFGL-TR-88-0150

HAC REF F4890

4

FLIGHT MODEL DISCHARGE SYSTEM

R.R. Robson and W.S. Williamson

Hughes Research Laboratories
3011 Malibu Canyon Road
Malibu, California 90265

June 1988

Scientific Report No. 4

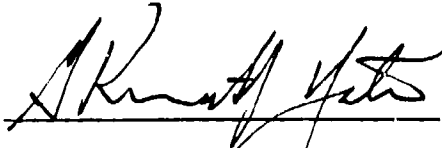

Approved for public release; distribution unlimited

AIR FORCE GEOPHYSICS LABORATORY
Air Force System Command
United States Air Force
Hanscom AFB, MA 01731

DTIC
ELECTE
NOV 21 1988
S D
C/E

88 11 21 010

" This technical report has been reviewed and is approved for publication"


G. KENNETH YATES
Contract Manager
for JOHN A. GAUDET, Lt Col, USAF
Branch Chief

FOR THE COMMANDER


RITA C. SAGALYN
Division Director

This report has been reviewed by the ESD Public Affairs Office (PA) and is releasable to the National Technical Information Service (NTIS).

Qualified requestors may obtain additional copies from the Defense Technical Information Center. All others should apply to the National Technical Information Service.

If your address has changed, or if you wish to be removed from the mailing list, or if the addressee is no longer employed by your organization, please notify AFGL/DAA, Hanscom AFB, MA 01731. This will assist us in maintaining a current mailing list.

Do not return copies of this report unless contractual obligations or notices on a specific document requires that it be returned.

TABLE OF CONTENTS

SECTION		PAGE
1	INTRODUCTION.....	1
2	FMDS TOTAL SYSTEM.....	3
	2.1 Overall System.....	5
	2.2 Components.....	7
3	ELECTROSTATIC ANALYZERS.....	21
4	SURFACE POTENTIAL MONITORS.....	35
	4.1 Basic SPM Design.....	35
	4.2 SPM Design Considerations.....	36
	4.3 SPM Flight Hardware.....	40
5	TRANSIENT PULSE MONITOR.....	43
6	CONTROLLER.....	49
7	PLASMA SOURCE.....	55
	7.1 Plasma Generator Design.....	55
	7.2 Test Results.....	58
	7.3 Contamination Measurements.....	70
8	SYSTEM THERMAL ANALYSIS.....	79
9	CONCLUSIONS.....	81
	BIBLIOGRAPHY.....	83



Accession For	
NTIS GRA&I	<input checked="" type="checkbox"/>
DTIC TAB	<input type="checkbox"/>
Unannounced	<input type="checkbox"/>
Justification	
By _____	
Distribution/	
Availability Codes	
Dist	Avail and/or Special
A-1	

LIST OF ILLUSTRATIONS

FIGURE		PAGE
1	Block Diagram of the FMDS.....	4
2	FMDS Flight Components Mounted on a 0.125-in-Thick Aluminum Plate.....	6
3	Shift in the Observed Ion and Electron Spectra Caused by Environmental Conditions Conducive to Charging and by Actual Charging of the Spacecraft.....	11
4	Charging Characteristics of a Shaded Dielectric Sensor.....	12
5	ESA S/N 001.....	24
6	Preliminary Test Sequence.....	25
7	Environmental Test Sequence.....	26
8	Flight Package Design for the SPM.....	37
9	SPM Input Electrode Assembly Showing the Discrete Resistor (5 Resistors in Series) Between the Input Electrode and Ground (Flying Lead).....	39
10	SPM Input Electrode Time Response Under Simulated Sunlight Conditions.....	41
11	A Complete SPM.....	42
12	A TPM Input Buffer Circuit Board.....	46
13	A Flight TPM Antenna Assembly.....	47
14	Controller I/O Board, S/N 001.....	50
15	ADC and I/O Board, S/N 001.....	51
16	Controller Electronics Box Without the Box End-Plate.....	52
17	Calibration of the ADC on ADC and I/O Board S/N 001.....	53
18	Simple Schematic of the Plasma Generator.....	57

LIST OF ILLUSTRATIONS (Continued)

FIGURE		PAGE
19	Cross Section of the Flight Plasma Generator.....	59
20	A Flight Plasma Generator in an Exploded Configuration.....	60
21	Stripchart Recording of the Keeper Voltage of Source S/N 003 During Initial and Unacceptable Operation (Contaminated Cathode and Insert).....	61
22	Stripchart Recording of the Keeper Voltage of Source S/N 003 After Elimination of the Contamination Problems, Showing Very Good Performance.....	63
23	Ion Emission Current as a Function of Keeper Current and Discharge Current.....	64
24	Total Input Power to the Source as a Function of Keeper Current and Discharge Current.....	65
25	Specific Ion Emission Current ($\mu\text{A/W}$) as a Function of Keeper Current and Discharge Current.....	66
26	Plasma Growth Electronics Board No. 2, S/N 001.....	69
27	Positions of the Contamination "Witness" Slides During the Plasma Generator Lifetest.....	71
28	Optical Transmission Loss of Contamination "Witness" Slide 3.....	72
29	Apparatus used in FMDS Spectroscopic Measurements.....	74

LIST OF TABLES

TABLE		PAGE
1	Summary of FMS Weights.....	8
2	Summary of FMDS Power Consumption.....	9
3	Electrostatic Analyzer Contractual Specifications and Respective Flight Design Parameters.....	14
4	Surface Potential Monitor Contractual Specifications and Respective Flight Design Parameters.....	15
5	Transient Pulse Monitor Contractual Specifications and Respective Flight Design Parameters.....	16
6	Controller Contractual Specifications and Respective Flight Design Parameters.....	17
7	Plasma Source Contractual Specifications and Respective Flight Design Parameters.....	18
8	FMDS System Contractual Specifications and Respective Flight Design Parameters.....	19
9	Energy Detection Characteristics of the ESAs	22
10	Summary of Performance Test Data (Normalized to Nominal Value) for ESA S/N 001.....	27
11	Summary of Bias Voltage vs Energy Channel Nominal Counts for Ion CEM.....	30
12	Nominal Counts Normalized to Ion CEM Bias = 0.....	31
13	Summary of Bias Voltage vs Energy Channel Nominal Counts for Electron CEM.....	32
14	Nominal Counts Normalized to Electron CEM Bias = 0.....	33
15	SPACECLAMP Plasma Generator Characteristics.....	56
16	Operating Points Illustrated in Figures.....	67

SECTION 1

INTRODUCTION

The objectives of the FMDS program are to design, develop, fabricate, test, and deliver two flight units of a satellite Flight Model Discharge System (FMDS). The FMDS is a stand-alone system capable of autonomous operation (except for power) that will monitor spacecraft potential, determine when spacecraft charging is present, and operate a discharge device to eliminate potentials and maintain the spacecraft in a neutral charge state. The FMDS is designed to be incorporated into the "housekeeping" function of any spacecraft subject to spacecraft charging. While full ground-command capability is retained for redundancy, only a "power on" command is required to activate the system. In addition to the capability for remote command override of its autonomous operation, the FMDS provides telemetry signals to monitor such functions as sensor outputs, controller "commands," plasma source operation, gas supply in the reservoir tank, and system state-of-health diagnostics (e.g., temperatures, voltages, and currents).

In the following technical discussion, we present the results of the fourth year's effort on the FMDS contractual program, which is being carried out at Hughes Research Laboratories in Malibu, California. An overview of the FMDS is presented, followed by an in-depth treatment of the significant technical developments of the past year. For an in-depth discussion of the operation and capabilities of the FMDS system, refer to Scientific Report No. 2.¹

This Page Intentionally Left Blank

SECTION 2

FLIGHT MODEL DISCHARGE SYSTEM TOTAL SYSTEM

The FMDS is a stand-alone system capable of autonomous operation (except for power) that monitors space-vehicle potential, determines when charging is present, and operates a discharge device to eliminate charge buildup and maintain the vehicle in a neutral charge state. The FMDS is designed to be incorporated into the "housekeeping" functions of any vehicle subject to spacecraft charging. While full ground-command capability is retained for redundancy, only a "power on" command is required to activate the system. It detects charging, operates to neutralize the charging, and returns to the passive mode when the charging hazard is no longer present.

The FMDS consists of three types of components:

- (1) Charging sensors:
 - Electrostatic Analyzers (ESAs). These sensors detect absolute charging relative to the ambient plasma in space.
 - Surface Potential Monitors (SPMs). These sensors determine differential charging relative to spacecraft ground.
 - Transient Pulse Monitor (TPM). This sensor detects the electromagnetic pulses generated by the onset of arcing.
- (2) An active discharge device (plasma source).
- (3) A control unit to interpret the sensor outputs, determine when and if charging is occurring, and control the discharge device.

A block diagram of the system is shown in Figure 1.

The controller incorporates comprehensive charging-detection algorithms that contain ground-alterable parameters to allow in-space refinement of FMDS operation. The controller incorporates redundant and fault-tolerant software to permit the FMDS to

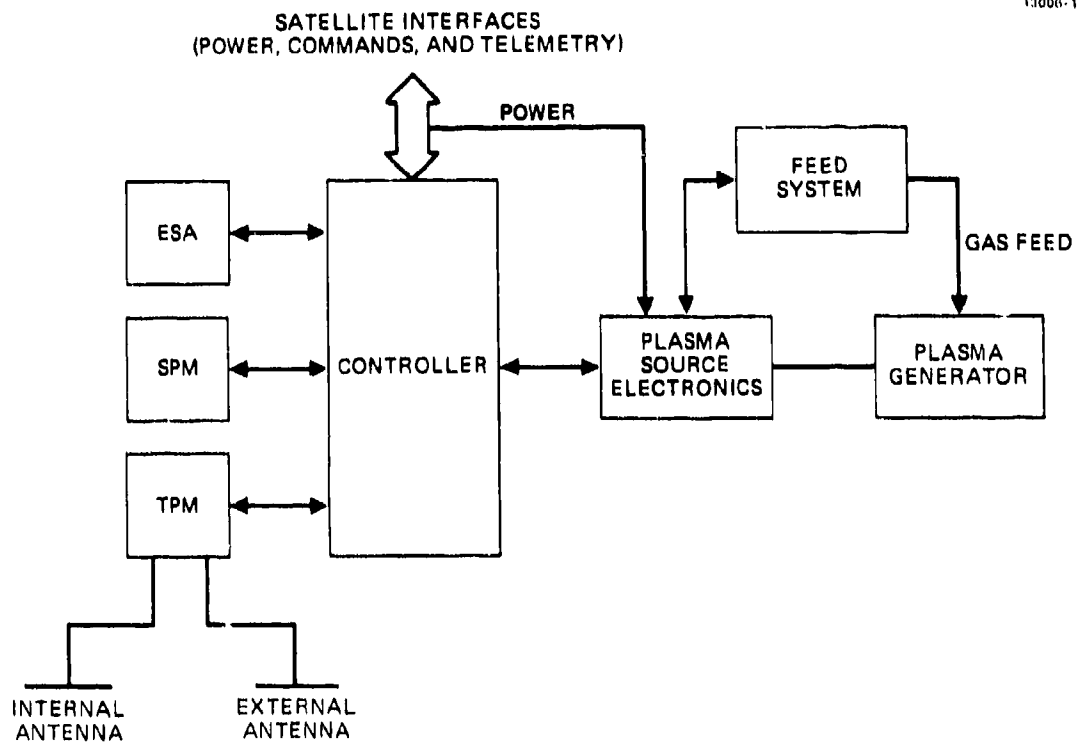


Figure 1. Block diagram of the FMDS.

continue operation in the face of specific faults or failures. In addition, it has the capability for ground- or remote-command override of its autonomous operation, and also provides telemetry signals to monitor such functions as sensor outputs, controller status flags, plasma source operation, gas supply pressure in the reservoir tank, temperatures, voltages, and currents.

The FMDS is ultimately intended for extended satellite operation at geosynchronous orbit; however, it is designed to withstand the launch and operating environments of both geosynchronous and Shuttle orbits. While the primary emphases are safety and reliability, low-operating and transient voltages are also considered to prevent Paschen breakdown and to minimize EMI.

2.1 OVERALL SYSTEM

Figure 2 is a photograph of the FMDS flight configuration, where the flight components are mounted to an aluminum base plate (for assembly purposes). The aluminum base plate will be replaced in the final hardware with a honeycomb-structure mounting plate to provide a simple lightweight and structurally sturdy interface with the host spacecraft. No attempt is made in this photograph to indicate the exact mechanical interface of the FMDS with the host spacecraft, because at this time a specific ride has not been determined. The structurally integrated design approach will also facilitate system testing in both laboratory vacuum chambers and environmental test fixtures (vibration, thermal/vacuum, etc.).

Because of the diversity of functions required of the various FMDS components, each element is packaged separately and attached separately to the common mounting plate. Maintaining separation between each of the components has the added advantage of facilitating substitution of upgraded component designs if such upgrades become available in the future.

The two SPMs and the ESAs are mounted on one end of the FMDS mounting plate to provide both maximal and similar exposure

MC17953

18296-6

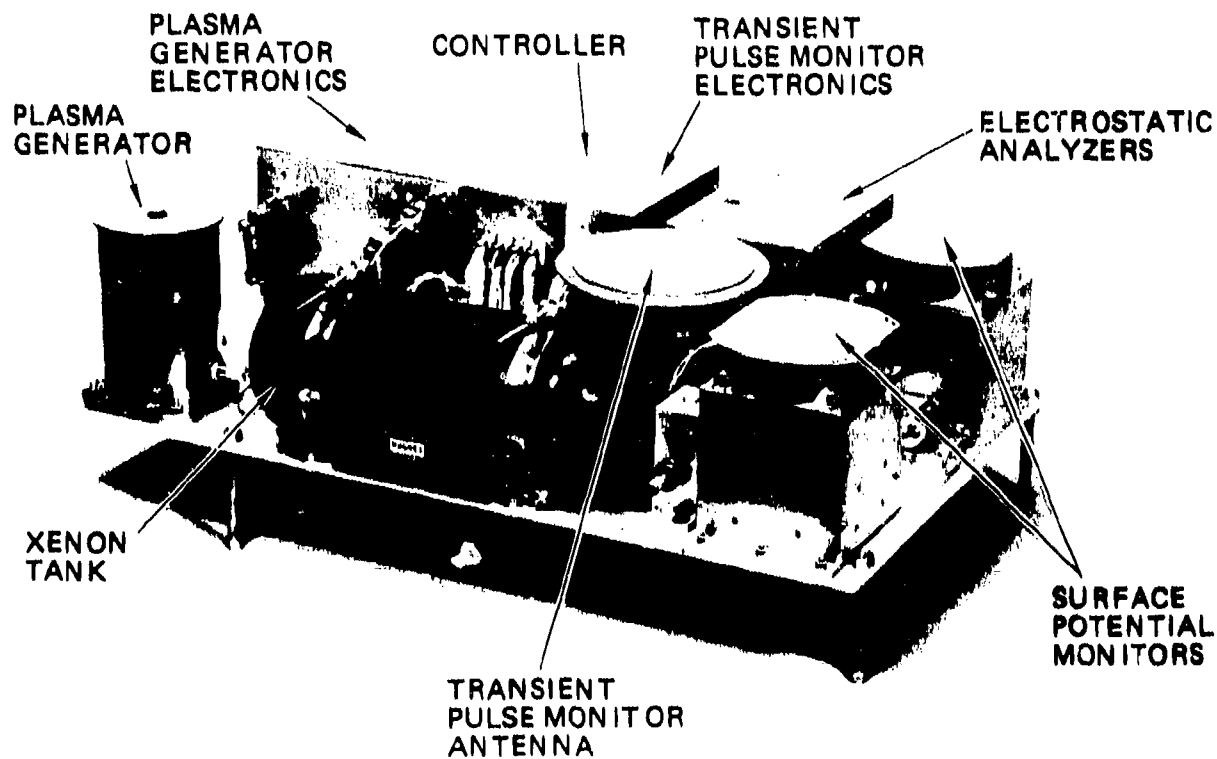


Figure 2. FMDS flight components mounted on a 0.125-in-thick aluminum plate.

of the sensors to incoming particle flux, while avoiding (as much as possible) any local distortions of electrostatic equipotentials that might be caused by other devices, such as the plasma source.

The plasma source is located at the other end of the FMDS, where it is farthest from the charged-particle entrance apertures of the ESAs; this will minimize the introduction of plasma-source-generated particles. In this location, the source is reasonably remote from both the ESAs and the SPMs.

The electronics packages for the plasma-generator, TPM, and controller; the SPMs; the ESAs; and the plasma generator are all at the same height. This uniformity allows adding a cover to the FMDS to form a ground plane and to provide a mounting surface for the TPM external antenna if the FMDS is mounted to the exterior of a spacecraft.

Inasmuch as the FMDS is intended for satellite use, minimizing weight, volume, and power is of utmost concern. The overall FMDS is estimated to weigh 21.7 kg (47.7 lb) (a 2.3 kg increase from the CDR estimate), and to consume less than 17.0 W (an increase of 3.3 W from the CDR estimate) when the plasma source is not activated, and less than 28.8 W when it is activated. FMDS weights and power consumption are summarized in Tables 1 and 2 respectively. The overall dimensions are 16.5 by 38.1 by 61 cm (6.5 by 15 by 24 in.).

2.2 COMPONENTS

The ESAs will measure the energy distribution (from 50 eV to 20 keV) of the particles incident upon the satellite. We expect this energy distribution to shift when the environmental conditions are conducive to spacecraft charging (caused by a change in the environmental conditions), there is a second apparent shift which is directly related to the potential of the satellite frame relative to the space potential. Because the ESAs are referenced to the satellite frame, and the particles originate with energies relative to space potential, any change

TABLE 1. Summary of FMDS Weights.

T9234-1

Unit	CDR Estimate		Latest Estimate		Contract Spec, lbs
	Mass, kg	Weight, lbs	Mass, kg	Weight, lbs	
ESA	2.7	6.0	1.88	4.15	6.0
SPM (2 Units)	1.4	3.0	2.35	5.20	3.0
TPM	1.6	3.5	1.82	4.02	3.0
Controller	1.7	3.7	1.43	3.15	—
Plasma Source	1.4	3.0	1.70	3.75	} 15.0
Source Electronics	2.0	4.4	4.18	9.18	
Feed System	4.2	9.2	4.14	9.12	
Harness	0.7	1.5	0.57	1.26	—
Thermal Control	0.9	2.0	0.00	0.00	—
Enclosure	2.2	4.8	2.98	6.56	—
FMDS Dry Mass	18.8	41.1	21.05	46.39	—
Xenon	0.6	1.3	0.60	1.30	—
FMDS at Launch	19.4	42.4	21.65	47.69	35.0

TABLE 2. Summary of FMDS Power Consumption.

T9234-2R1

Unit	CDR Estimate		Latest Estimate		Contract Spec, W
	Source Off, W	Source On, W	Source Off, W	Source On, W	
ESA	1.25	1.25	1.49	1.49	1.25
SPM (2 Units)	1.0	1.0	1.00	1.00	2.0
TPM	4.0	4.0	6.44	6.44	3.0
Controller	4.0	4.0	2.90	2.90	(4.0)
Plasma Source	0.0	13.7	0.00	11.80	(25.0)
Housekeeping Inverter	3.4	4.1	5.14	5.14	—
FMDS	13.7	28.1	16.97	28.77	35.0
FMDS Contract Spec	10.0	35.0	10.0	35.0	35.0

() = Inferred

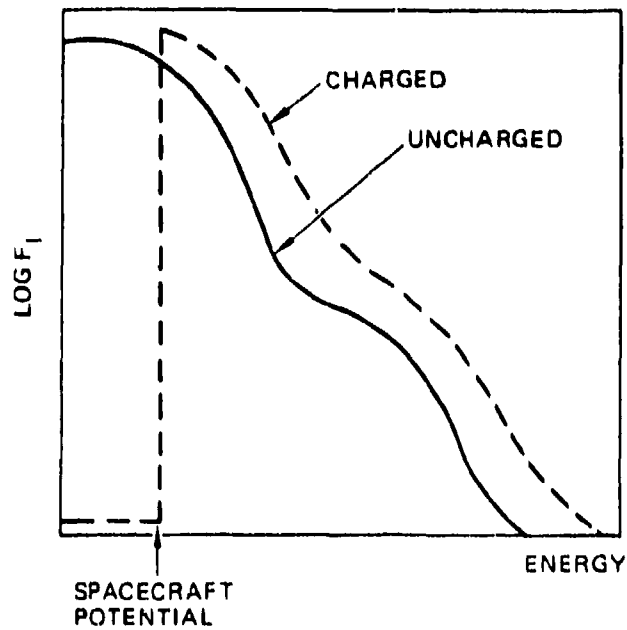
in the potential of the satellite frame will appear as a change in the particle-energy distributions. Algorithms in the controller will detect the shift in the particle-energy distributions (Figure 3) in order to (1) provide an early warning that the environmental conditions are conducive to spacecraft charging (by detection of electrons), and (2) detect that charging of the satellite frame has exceeded a threshold level (by ion detection) and provide a signal to turn on the plasma source.

The SPMs will detect the onset of differential charging of the satellite dielectric surfaces. When the satellite is in sunlight and charging conditions exist, the isolated dielectric surfaces that are shaded will charge much faster than the satellite frame because of the absence of the neutralizing effect of photo-emission from these shaded surfaces (Figure 4). Therefore, through measurement of the potential on the surface of a shaded dielectric sensor, differential charging can be detected quickly and prior to the detection of satellite-frame charging by the ESA. When the satellite is in eclipse, however, satellite-frame charging occurs faster than differential charging (Figure 4). In this circumstance the ESA will be the prime detector.

The TPM will detect electrical discharges that occur on the surface of the satellite as a result of differential charging. A floating-plate sensor is employed to pick up radiated electric fields caused by these discharges. If electrical discharges are occurring, the implication is that the satellite is charged up, that the plasma generator should be turned on, and that the other sensors have failed to detect the charging. The TPM has ground-adjustable parameters and can be commanded to ignore transients occurring within 1 s following receipt of a command by the spacecraft. The TPM is designed to avoid false arc-discharging alarms.

The controller provides for autonomous control of the FMDS relative to the remainder of the satellite. This device also ties together the other units of the FMDS. The brain of the

ION SPECTRUM



ELECTRON SPECTRUM

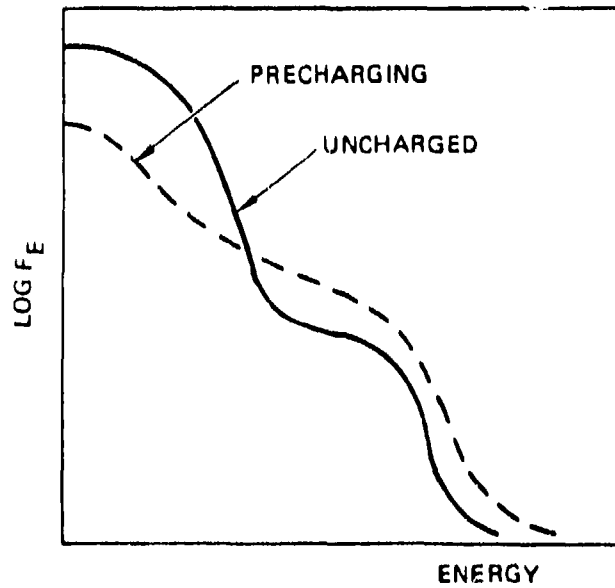


Figure 3. Shift in the observed ion and electron spectra caused by environmental conditions conducive to charging and by actual charging of the spacecraft.

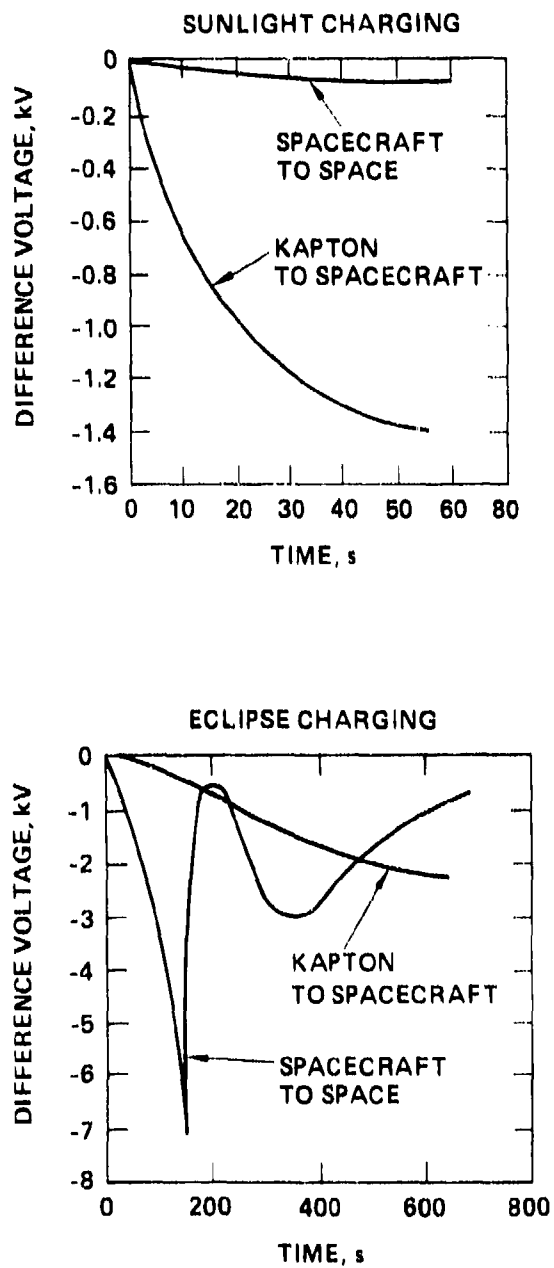


Figure 4. Charging characteristics of a shaded dielectric sensor.

controller is a microprocessor that contains the algorithms necessary to interpret the data from the sensors and command the plasma generator to turn ON when spacecraft charging is occurring, and then turn OFF when it is no longer required. The plasma generator is turned OFF after a programmable time-out (when the emission current from the plasma generator has been less than a threshold value for a specified period of time) and when the ambient electron environment returns to a quiescent condition. The controller also provides the command and telemetry interface with the satellite.

The plasma generator emits xenon and hydrogen ions and electrons in sufficient quantity (>1 mA) to bathe the satellite in a conductive low-energy (<50 -eV) plasma. This conductive plasma will drain the charge from dielectric surfaces and also form a "plasma bridge" to the surrounding natural space-plasma environment. The plasma generator is capable of igniting in <1 s, operating for 1200 h, and executing 1000 ON/OFF cycles. It requires three power supplies and a gas-feed system consisting of a xenon/hydrogen (90% to 10%) storage tank, a pressure regulator, valves, and a flow regulator.

Tables 3 through 8 list the major contractual specifications for the ESAs, SPMs, TPM, controller, plasma source, and system, respectively. The respective parameters of the actual flight design are also listed in these tables.

TABLE 3. Electrostatic Analyzer Contractual Specifications and Respective Flight Design Parameters.

14881-17R5

CONTRACTUAL SPECS	DESIGN
ION AND ELECTRON SPECTRA < 100 eV TO 20 keV	50 eV TO 20 keV
GEOMETRIC FACTOR $\approx 10^{-5}$ TO 10^{-4} cm ² - SR	6×10^{-4} cm ² - SR
≥ 8 ENERGY CHANNELS	16 CHANNELS
$\leq 2\%$ OVERLAP AT FWHM	$\leq 2\%$ OVERLAP--NO GAPS
SWEEPS OF 2, 5, AND 10 s	SWEEPS OF 4, 8, 16, AND 32 s
VOLTAGES SETTLED TO 95% BEFORE COUNTING	VOLTAGES SETTLED TO $\geq 95\%$ BEFORE COUNTING
GRID TO REPEL PLASMA SOURCE IONS AND ELECTRONS (< 50 eV)	GRID BIASED AT 50 V
SUN SENSOR TO PROTECT CEM	SUN SENSOR
CMD OVERRIDE OF SUN SENSOR	CMD OVERRIDE
REDUCE UV SCATTERING	SANDBLASTED PLATES
COMMANDABLE CEM BIAS	COMMANDABLE BIAS (8 LEVELS)
THREE-YEAR ON ORBIT LIFE	DESIGNED FOR THREE-YEAR OPERATIONAL LIFE
TELEMETRY	ACCUMULATED COUNTS, ENERGY CHANNEL, STATUS, AND DIAGNOSTICS
< 1.25 W	≤ 1.50 W
< 6 lb	≤ 4.2 lb

TABLE 4. Surface Potential Monitor Contractual Specifications and Respective Flight Design Parameters.

14881-18R3

CONTRACTUAL SPECS	DESIGN
DIELECTRIC SURFACE POTENTIAL MEASURED WITH ELECTRIC FIELD SENSOR	VIBRATING ELECTRODE ELECTROSTATIC VOLTMETER
POTENTIAL AND POLARITY FROM 100 V TO 20 kV	DUAL RANGE: ± 2 kV ± 20 kV
TWO DIFFERENT DIELECTRICS IN FLIGHT	TWO INSTRUMENTS WITH DIFFERENT DIELECTRICS
CHOICE OF SIX DIFFERENT DIELECTRICS	CHANGE SENSING PLATE TO CHANGE DIELECTRICS
TELEMETRY	SURFACE POTENTIAL, RANGE, DIAGNOSTICS
< 2 W	≈ 1 W (2 UNITS)
< 3 lb	≈ 5.2 lb (2 UNITS)

TABLE 5. Transient Pulse Monitor Contractual Specifications and Respective Flight Design Parameters.

14881-19R5

CONTRACTUAL SPECS	DESIGN
DIPOLE SENSOR	MONOPOLE (123 cm ² PLATE)
MEASURE RADIATED ELECTROMAGNETIC PULSES	MEASURE ELECTROSTATIC PULSES
MULTIPLE THRESHOLD LEVELS	8-BIT DAC
PARAMETERS MEASURED/1s <ul style="list-style-type: none"> - MAX POSITIVE PEAK AMPLITUDE - MAX NEGATIVE PEAK AMPLITUDE - POSITIVE INTEGRAL - NEGATIVE INTEGRAL - PULSE WIDTH - NUMBER OF PULSES 	PARAMETERS MEASURED/4s <ul style="list-style-type: none"> - POSITIVE PEAK AMPLITUDE/PULSE - NEGATIVE PEAK AMPLITUDE/PULSE - INTEGRALS NOT MEASURED - PULSE WIDTH/PULSE - PULSES/4s
10 V/M TO 10 kV/m FIELD STRENGTH	10 V/m TO 10 kV/m
10 ns TO 10 μs PULSE WIDTHS	20 ns TO 10 μs
1 COUNT/ms MAX	1 COUNT/5ms
TELEMETRY	PARAMETERS MEASURED AND DIAGNOSTICS
< 3 W	< 6.5 W
< 3 lb	< 4.1 lb

**TABLE 6. Controller Contractual Specifications and
Respective Flight Design Parameters.**

192346

Contract Specs	Design
Provide autonomous operation of FMDS	Autonomous operation
Determine if threshold levels of charging have been exceeded	Charging above threshold will be detected
Turn on plasma source and operate for 5, 10, 30, or 60 min	Turn on and control plasma source. Turn off based on time (30, 60, 90, 120 min) and/or environmental conditions
Detect with 98% reliability <ul style="list-style-type: none"> - 95% of cases for charging ≥ 500 V - 100% of cases for charging ≥ 1000 V 	Designed to meet based on SC9 data
Commandable threshold charging levels of 200, 500, 1000, and 2000 V	Same
Spacecraft arcing to activate plasma source	Arcing will activate plasma source
EMI pulses within 1 s of spacecraft command to be ignored	Ability to blank TPM for 1 s (requires signal from spacecraft)
External command adjustment of TPM algorithm	All algorithms will be adjustable via external command
External commanding of plasma source	Manual operation of complete FMDS
Telemetry	Status and diagnostics
Design to include considerations of radiation hardening	Hardened to 5×10^5 rads (flight)
Redundancy	Critical parameters stored in three locations (majority voting)
Excess capacity	Excess memory and I/O

**TABLE 7. Plasma Source Contractual Specifications
and Respective Flight Design Parameters.**

14881-20R4

CONTRACTUAL SPECS	DESIGN
< 50 eV NEUTRAL PLASMA	< 40 eV
IONS FROM A NOBLE GAS	90% XENON-10% HYDROGEN
10 μ A, 100 μ A, AND 1 mA ION CURRENT LEVELS (SELECTABLE)	< 200 μ A TO > 1 mA, 4 SETPOINTS FOR DISCHARGE AND KEEPER
\leq 10s IGNITION	\leq 1s
1200 HOURS OPERATION	\geq 1200 hr
1000 ON-OFF CYCLES	\geq 1000 CYCLES
< 25 W	\leq 10 W OPERATING \leq 20 W CONDITIONING
< 15 lb	< 22.5 lb DRY
BLOW-OFF COVER	REMOVE-BEFORE-LAUNCH COVER
TELEMETRY	EMISSION CURRENT AND DIAGNOSTICS

**TABLE 8. FMDS System Contractual Specifications
and Respective Flight Design Parameters.**

T9234-8

Contractual Specs	Design
Low-energy plasma within 30s of exceeding a charging threshold	Same except for ESA 16-s sweep which requires 38s
Analog telemetry outputs between 0.00 and 5.10 V	No analog signals to satellite
Digital commands and telemetry TTL compatible	TTL compatible and optically isolated
All ground returns self contain and isolated by \geq megohm	Designed to meet - single ground point philosophy
Permanent magnetic fields ≤ 100 nT at 1 meter in any direction	Designed to meet
Mating connectors to be furnished	Mating connectors will be furnished
No cadmium-plated connectors or other hardware	No cadmium anywhere
<35 lbs.	46.5 lbs. dry 48.0 lbs. at launch
<10 W with plasma source off	17.0 W with source off 29.0 W with source on
Power profile to be provided	Power profile will be measured and provided
High-rel parts for >3 yr life in deep space orbit	Rad-hard Class-B parts
Thermal models to be provided	Analytical thermal models will be provided
Mass models to be provided - both analytical models and hardware simulators	Analytical mass models and hardware mass simulators will be provided
Electrical simulators to be provided	Electrical simulators will be provided
Ground support equipment to be provided - command/telemetry and power source	Ground support equipment will be provided - command/telemetry, power source, and vacuum pump
EMI: designed to meet MIL-STD-461B and MIL-STD 1541	Designed to meet
Shall meet shuttle safety requirements - NASA handbook 1700.7A, JSC 11123 and JSC 13830	Designed to meet
Acceptance tests to be performed in accordance with MIL-STD-1540A	Designed to meet

TABLE 8. Continued.

T9234-8

Contractual Specs	Design
Random Vibration: Frequency (Hz) PSD (g^2/Hz) 20 0.004 20-37.5 +12 dB/octave 37.5-90 0.050 90-200 +4 dB/octave 200-700 0.150 700-2000 -4 dB/octave Composite 13.7 g rms Duration of 2 min along each of 3 orthogonal axis	Designed to meet
Sine survey: 0.5 to 1.0 g 15 to 100 Hz One sweep up and down in each axis at 2 octaves/min	Designed to meet
Transient shock: 25 g, 11 ms, half-sine pulse along each axis	Designed to meet
Thermal vacuum: $\geq 10^{-5}$ Torr -24°C to $+61^\circ\text{C}$ 12 h at the low and high temperature levels	Designed to meet
Thermal cycling: Ambient pressure -24°C to $+61^\circ\text{C}$ ≥ 8 cycles with 2 h dwell at low and high temperature, transitions at $\geq 3^\circ\text{C}/\text{min}$	Designed to meet
Burn-in: Ambient pressure -24°C to $+61^\circ\text{C}$ ≥ 18 total cycles including those above	Designed to meet
Depressurization/repressurization: Shuttle profile JSC 07700 Vol. XIV Attachment 1, Rev. G	Designed to meet

SECTION 3

ELECTROSTATIC ANALYZERS

The FMDS incorporates ESAs to measure the distribution of ion and electron energies incident on the spacecraft. The ESAs are important to the FMDS charging-detection function because, of the instruments specified for FMDS, they alone can detect the onset of eclipse charging. (The SPMS respond too slowly when the spacecraft is in darkness.) The data can be analyzed to determine the actual vehicle potential (i.e., frame potential relative to space potential), rather than the dielectric-surface potentials monitored by the SPMS. In addition to these important charging-detection attributes, the ESAs provide valuable scientific information.

The ESAs employed on the FMDS are configured with short-cylindrical section sensors. Instruments of this type have been used in physics experiments since the turn of the century, and similar devices have been flown on many spacecraft. The FMDS instrument incorporates 16 channels and fast sweep times (4, 8, 16, or 32 s) in order to provide the rapid reaction time required in the FMDS mission. The energy detection characteristics of the ESAs are shown in Table 9.

The ESAs for the FMDS are being provided by Panametrics Inc. of Waltham, MA, under subcontract. The basic design of this instrument has not changed during the past 12 months, and Scientific Report No. 2¹ should be consulted for further details. An oscillation problem was discovered in the flight hardware when the electronics was integrated with the detector heads. The oscillations occurred at the output of the high gain preamps in the detector heads and caused the electronics to record extra counts. Additional shielding and a ground plane (on the preamp printed wiring board) were added, and cured this problem.

TABLE 9. Energy Detection Characteristics of the ESAs.

14861--25R2

CHANNEL NUMBER	ENERGIES IN eV		
	E (LOW)	E (HIGH)	E (AVERAGE)
0	BACKGROUND CHANNEL		
1	50	75	62
2	75	111	93
3	111	166	138
4	166	247	206
5	247	368	308
6	368	549	459
7	549	819	684
8	819	1221	1020
9	1221	1821	1521
10	1821	2714	2267
11	2714	4047	3381
12	4047	6034	5041
13	6034	8997	7516
14	8997	13414	11205
15	13414	20000	16707
GEOMETRIC FACTOR $6 \times 10^{-4} \text{ cm}^2 - \text{sr}$ (CAN BE MADE SMALLER)			
INTRINSIC ENERGY RESOLUTION $\Delta E (\text{FWHM})/E (\text{AVERAGE}) = 39\%$			

The first flight unit (Figure 5) has successfully completed all acceptance and environmental qualification tests and has been delivered to Hughes. Figure 6 shows the preliminary test sequence and Figure 7 the environmental test sequence performed on the unit. A summary of the performance test data (normalized to nominal value) throughout the environmental qualification tests is presented in Table 10. The table also lists the tolerance (from the nominal value) that is considered acceptable for each parameter. None of the parameters ever exceed the tolerances.

Table 11 is a summary of the energy channel nominal counts vs CEM bias (Channel Electron Multiplier bias) for the ion channel using a H-3 beta source. Nominal count is calculated as the midpoint between the minimum and maximum counts for each energy channel for all the data taken during testing. Table 12 shows the nominal counts normalized to the CEM bias level 0. The first eight energy channels (0 through 7) have relatively high counts (Table 11) and therefore good statistics. The averages of the normalized counts for energy channels 0 through 7 at each CEM bias level are also listed in Table 12. These averages are approximately linear, with a slowly increasing slope as the bias level increases. These data represent operation within the plateau region of the CEM efficiency curve and below the noise region, which is the criterion for proper operation of the CEM.

Table 13 is a summary of the energy channel nominal counts vs CEM bias for the electron channel using a Ni-63 beta source. Nominal count is calculated as the midpoint between the minimum and maximum counts for each energy channel for all the data taken during testing. Table 14 shows the nominal counts normalized to the CEM bias level 0. The last six energy channels (10 through 15) have relatively high counts (Table 13) and therefore good statistics. The averages of the normalized counts for energy channels 10 through 15 at each CEM bias level

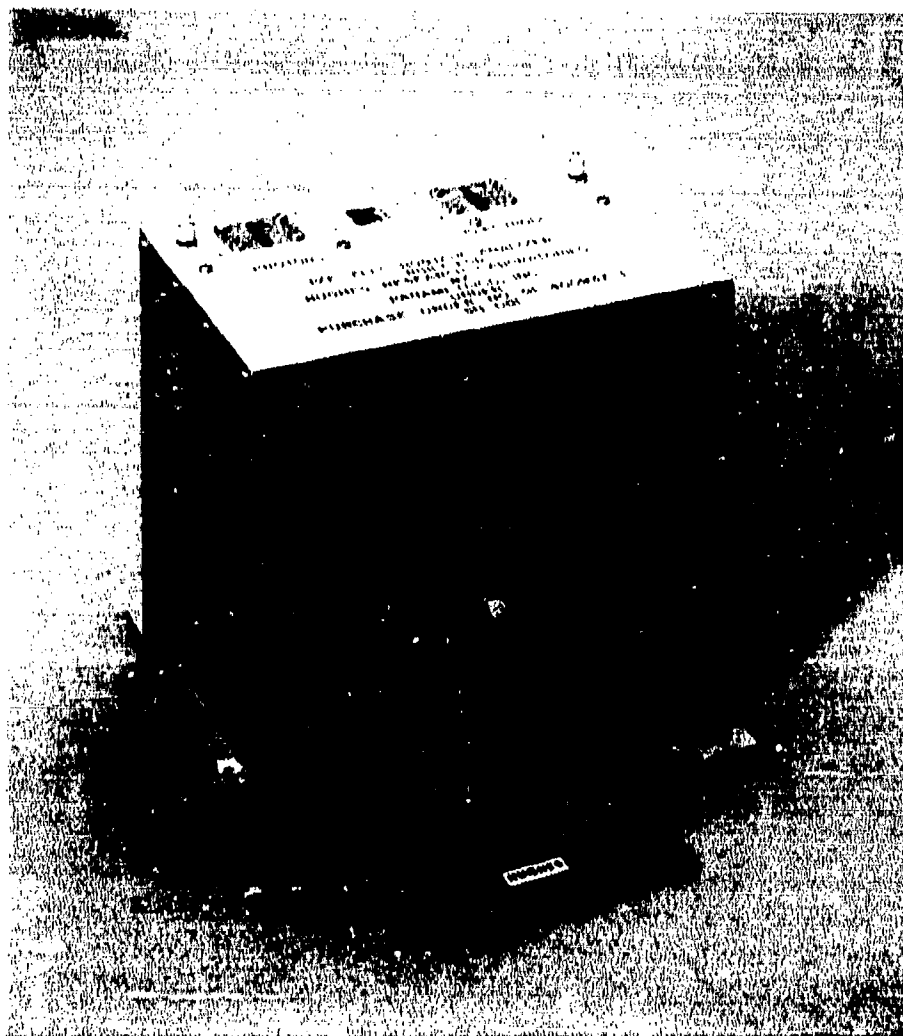


Figure 5. ESA S/N 001.

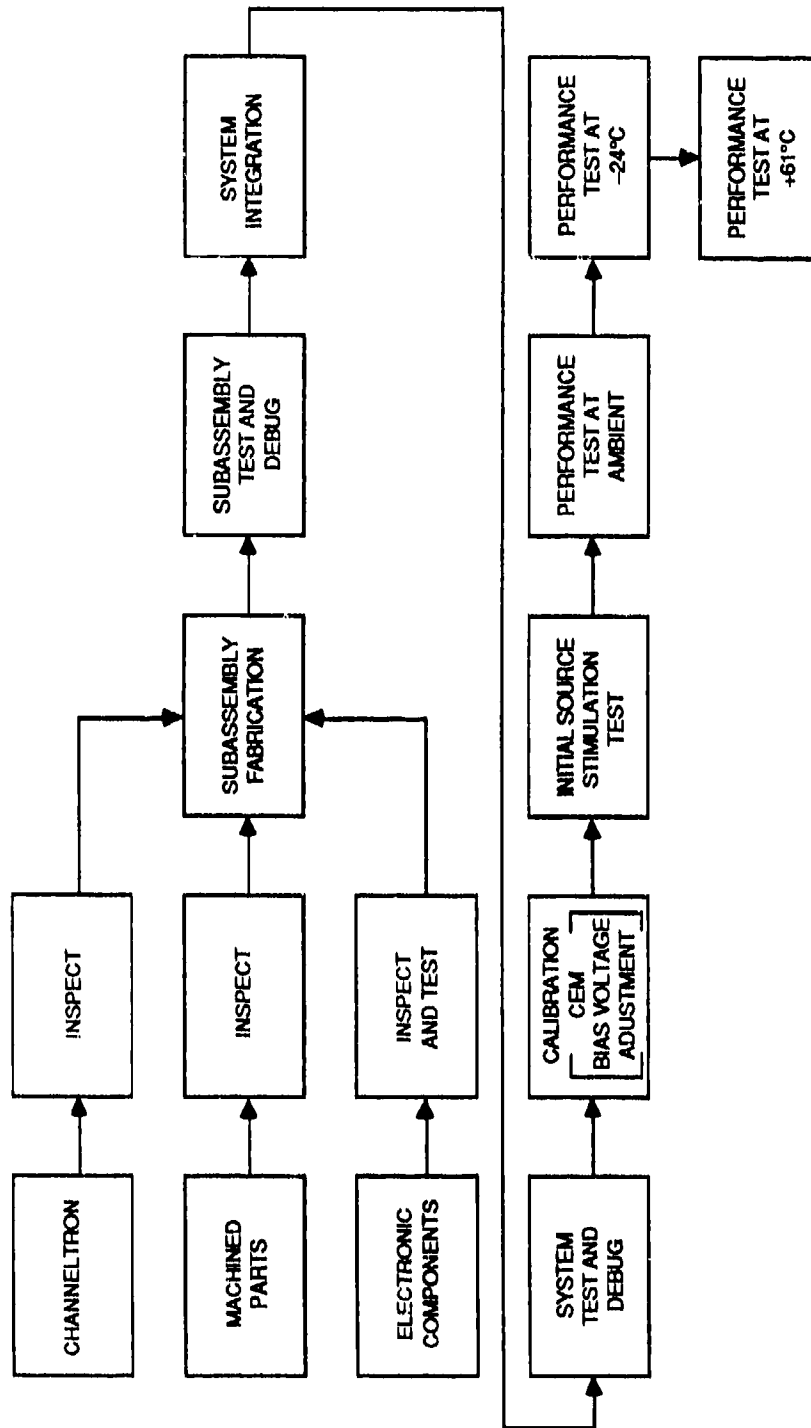


Figure 6. Preliminary test sequence.

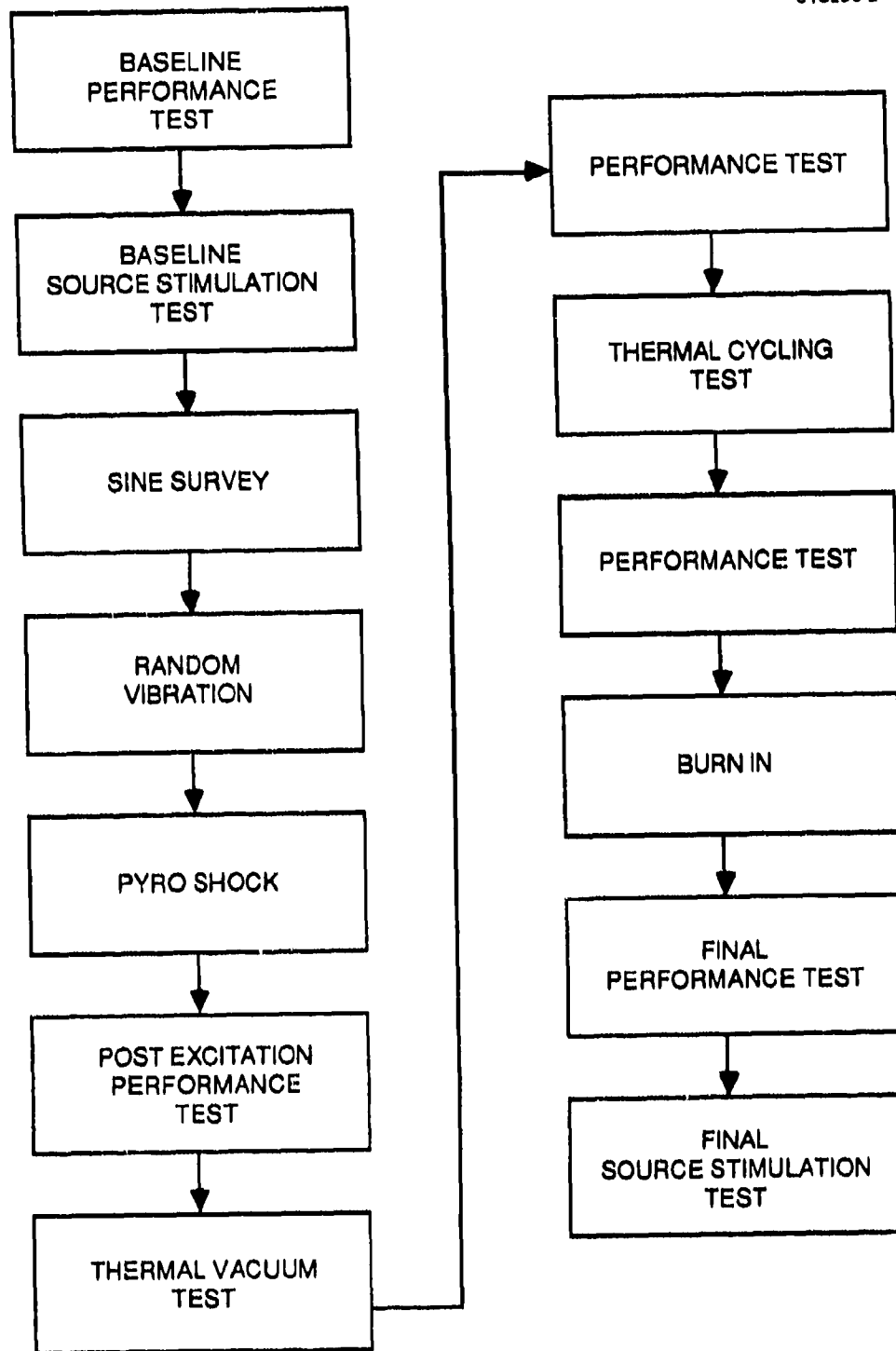


Figure 7. Environmental test sequence.

TABLE 10. Summary of Performance Test Data (Normalized to Nominal Value) for ESA S/N 001.

T9234-10

Analogue Monitor	Nominal Value	Tolerance	Pre-Prelim	Prelim -24	Prelim +61	Base-line	Post Excit	Th Vac Ambie.	Th Vac -24 #1	Th Vac -24 #2	Th Vac +61 #1	Th Vac +61 #2	Pos Th Vacuum	Pre Th Cycle	Pos Th Cycle	Pre Burn	Post Burn	Final
+3500V	1.00	0.03	1.00	0.99	1.00	1.00	0.99	1.00	1.00	1.00	1.00	1.00	1.00	1.00	1.00	1.00	0.99	1.00
+2500V	1.00	0.03	1.00	1.00	1.00	1.00	1.00	1.00	1.00	1.00	1.00	1.00	1.00	1.00	1.00	1.00	1.00	1.00
+/- 500V	1.00	0.03	1.00	1.00	1.00	1.00	1.00	1.00	1.00	1.00	1.00	1.00	1.00	1.00	1.00	1.00	1.00	1.00
REF V	1.00	0.03	1.00	1.00	1.00	1.00	1.00	1.00	1.00	1.00	1.00	1.00	1.00	1.00	1.00	1.00	1.00	1.00
+20V TP	1.00	0.03	1.00	1.00	1.00	1.00	1.00	1.00	1.00	1.00	0.99	0.99	1.00	1.00	1.00	1.00	1.00	1.00
+15V TP	1.00	0.03	1.00	1.00	1.00	1.00	1.00	1.00	1.00	1.00	0.99	0.99	1.00	1.00	1.00	1.00	1.00	1.01
+10V TP	1.00	0.03	0.99	1.00	1.00	1.00	1.00	1.00	0.99	1.00	1.00	1.00	0.99	1.00	0.99	1.00	0.99	1.00
+5V TP	1.00	0.03	1.00	0.99	1.00	1.00	1.00	1.00	1.00	0.99	1.00	1.00	1.00	1.00	1.00	1.00	1.00	1.00
-5V TP	1.00	0.03	1.00	1.00	1.00	1.00	1.00	1.00	1.00	1.00	1.00	1.00	1.00	1.00	1.00	1.00	1.00	1.00
-15V TP	1.00	0.03	1.00	1.00	1.00	1.00	1.00	1.00	1.00	1.00	1.00	1.00	1.00	1.00	1.00	1.00	1.00	1.00
TEMP AMB	1.00	0.03	1.00	1.02	1.00	1.00	1.00	1.00	0.98	0.98	1.00	0.99	1.00	1.00	1.00	1.00	0.99	1.00
TEMP +61	1.00	0.03	1.00	1.00	1.00	1.00	1.00	1.00	1.00	1.00	1.00	1.00	1.00	1.00	1.00	1.00	1.00	1.00
Int. min @ 24V	1.00	0.10	1.02	0.98	1.02	0.98	0.98	0.96	0.98	0.94	1.02	1.06	0.94	0.94	0.94	0.94	0.94	0.94
Int. max @ 24V	1.00	0.10	1.00	0.95	1.00	0.98	0.97	0.97	0.97	0.93	1.02	1.07	0.95	0.95	0.95	0.95	0.95	0.95
Int. min @ 28V	1.00	0.10	1.02	1.00	1.05	1.00	1.00	0.98	1.00	0.98	1.02	1.05	0.98	0.98	0.95	0.95	0.95	0.95
Int. max @ 28V	1.00	0.10	1.00	0.98	1.02	0.98	0.98	0.96	0.98	0.96	1.02	1.06	0.96	0.96	0.96	0.96	0.94	0.94
Int. min @ 32V	1.00	0.10	1.03	1.00	1.05	1.00	1.00	0.97	1.00	0.97	1.00	1.03	0.97	0.97	0.95	0.95	0.97	0.95
Int. max @ 32V	1.00	0.10	0.98	0.98	1.02	0.98	0.98	0.95	0.98	0.95	1.00	1.05	0.98	0.95	0.95	0.95	0.95	0.95
Pwr. min @ 24V	1.00	0.10	1.02	0.98	1.02	0.98	0.98	0.96	0.98	0.93	1.02	1.06	0.93	0.93	0.93	0.93	0.93	0.93
Pwr. max @ 24V	1.00	0.10	0.99	0.94	0.99	0.98	0.96	0.96	0.96	0.93	1.01	1.05	0.94	0.94	0.94	0.94	0.94	0.94
Pwr. min @ 28V	1.00	0.10	1.02	0.99	1.04	0.99	0.98	0.98	0.99	0.98	1.02	1.04	0.98	0.98	0.95	0.95	0.95	0.95
Pwr. max @ 28V	1.00	0.10	0.99	0.97	1.01	0.97	0.97	0.96	0.97	0.96	1.01	1.05	0.96	0.96	0.96	0.96	0.93	0.93
Pwr. min @ 32V	1.00	0.10	1.02	1.00	1.05	1.00	1.00	0.97	1.00	0.97	1.00	1.02	0.97	0.97	0.94	0.94	0.97	0.94
Pwr. max @ 32V	1.00	0.10	0.97	0.97	1.02	0.97	0.97	0.95	0.97	0.95	1.00	1.04	0.97	0.95	0.95	0.95	0.95	0.95

TABLE 10. Continued.

T9234-10

Electron CEM Bias Voltage (+3500V Monitor)													
e CEM Bias Level	Nominal Value	Tolerance	Pre-Prelim	Prelim -24	Prelim +61	Base-line	Post Excit	Th Vac Ambe.	Th Vac -24 #1	Th Vac -24 #2	Th Vac +61 #1	Th Vac +61 #2	Pos Th Vacuum
0	1.00	0.03	1.01	1.00	1.00	1.00	1.01	1.00	0.99	0.99	1.00	1.00	1.00
1	1.00	0.03	1.00	1.00	1.00	1.00	1.00	1.00	1.00	1.00	1.00	1.00	1.00
2	1.00	0.03	1.01	1.00	1.00	1.00	1.00	1.00	1.00	1.00	0.99	1.00	1.00
3	1.00	0.03	1.00	1.00	1.00	0.99	0.99	1.00	1.00	1.00	0.99	1.00	1.00
4	1.00	0.03	1.00	1.00	1.00	1.00	1.00	1.00	1.00	1.00	0.99	1.00	1.00
5	1.00	0.03	1.00	1.00	1.00	1.00	1.00	1.00	1.00	1.00	1.00	1.00	1.00
6	1.00	0.03	0.99	1.01	1.00	0.99	1.00	0.99	0.99	0.99	1.00	0.99	1.00
7	1.00	0.03	1.00	1.00	1.01	1.00	1.00	1.00	1.00	1.00	0.99	1.00	1.00
8	1.00	0.03	1.01	1.00	1.00	1.00	1.00	1.00	1.00	0.99	1.00	1.00	1.01
Proton CEM Bias Voltage (+2500V Monitor)													
p CEM Bias Level													
0	1.00	0.03	1.00	1.00	1.00	1.00	1.00	1.00	1.00	1.00	1.00	1.00	1.00
1	1.00	0.03	1.00	1.00	1.00	1.00	0.99	1.00	0.99	1.00	0.99	1.00	1.00
2	1.00	0.03	1.00	1.00	1.00	1.00	1.00	1.00	1.00	1.00	1.00	1.00	1.00
3	1.00	0.03	1.01	1.00	1.00	1.00	1.00	0.99	1.01	1.00	0.99	1.00	1.00
4	1.00	0.03	1.00	1.00	1.00	1.00	1.00	1.00	1.00	1.00	0.99	1.00	1.00
5	1.00	0.03	0.99	1.01	1.00	1.00	1.00	1.01	1.00	1.01	1.00	1.00	1.01
6	1.00	0.03	1.00	1.00	1.00	1.00	1.00	1.00	1.00	1.00	1.00	1.00	1.00
7	1.00	0.03	1.00	1.00	1.00	0.99	1.00	1.00	1.00	1.01	0.99	1.00	1.00
8	1.00	0.03	1.00	1.00	1.00	1.00	1.00	1.00	1.00	1.00	1.00	1.00	1.00

TABLE 10. Continued.

Sweep Voltage Monitor																		
Energy Channel	Nominal Value	Tolerance	Pre-Prelim	Prelim -24	Prelim +61	Base-line	Post-Exit	Th Vac Ambie	Th Vac -24 #1	Th Vac -24 #2	Th Vac +61 #1	Th Vac +61 #2	Pos Th Vacuum	Pre Th Cycle	Pos Th Cycle	Pre Burn	Post Burn	Final
0	1.00	3.00	2.00	1.00	1.00	1.00	1.00	2.00	1.00	1.00	2.00	1.00	1.00	1.00	1.00	1.00	0.00	1.00
1	1.00	0.56	0.75	1.00	1.00	1.00	1.00	1.00	1.00	1.00	1.00	1.00	0.75	0.75	1.00	1.00	1.00	1.00
2	1.00	0.50	0.80	0.80	1.00	1.00	1.00	1.00	1.00	0.80	1.00	0.80	0.80	0.80	1.00	1.00	0.80	0.80
3	1.00	0.50	1.00	1.00	1.20	1.20	1.00	1.00	1.00	1.20	1.00	1.00	1.00	1.00	1.20	1.20	0.80	1.00
4	1.00	0.38	1.00	1.13	1.00	1.00	0.88	0.88	1.13	1.13	1.00	1.13	0.91	1.00	0.88	1.00	1.00	1.00
5	1.00	0.31	1.09	1.09	1.09	1.09	0.91	1.09	1.00	1.09	1.00	1.09	0.91	1.00	1.09	1.09	1.00	1.09
6	1.00	0.25	1.00	1.07	1.00	1.00	1.07	1.07	1.00	0.87	0.93	1.00	1.00	1.00	0.93	1.00	1.00	0.93
7	1.00	0.19	1.00	1.00	1.00	0.95	1.05	1.05	0.95	0.95	1.00	1.00	1.00	1.00	1.05	1.00	1.00	1.00
8	1.00	0.14	0.97	0.94	0.94	1.00	0.97	0.97	0.94	0.97	0.97	0.94	0.97	0.94	1.06	1.00	0.97	0.97
9	1.00	0.10	0.98	0.96	1.00	1.02	1.00	1.00	1.00	0.96	0.96	0.96	1.00	0.96	0.98	1.00	1.00	1.00
10	1.00	0.07	0.99	0.99	0.99	1.01	1.00	0.99	0.99	0.99	0.99	0.99	0.99	0.99	0.99	0.99	0.99	0.99
11	1.00	0.05	1.00	1.00	1.00	1.00	1.01	1.00	1.00	1.00	0.99	1.00	1.00	1.00	1.00	1.00	1.00	1.00
12	1.00	0.03	0.99	0.99	0.99	0.99	1.00	0.99	0.99	0.99	0.99	0.99	0.99	0.99	0.99	0.99	0.99	0.99
13	1.00	0.02	1.00	1.00	1.00	1.00	1.00	1.00	1.00	1.00	1.00	1.00	1.00	1.00	1.00	1.00	1.00	1.00
14	1.00	0.02	1.00	1.00	1.00	0.99	1.00	1.00	1.00	1.00	0.99	1.00	1.00	1.00	0.99	1.00	1.00	1.00
15	1.00	0.01	1.00	1.00	1.00	1.00	1.00	1.00	1.00	1.00	1.00	1.00	1.00	1.00	1.00	1.00	1.00	1.00
0	1.00	3.00	0.50	1.50	1.00	0.00	0.50	0.50	0.50	1.00	1.00	1.00	0.00	0.00	0.50	0.50	1.00	0.50
Thresholding Firing Level																		
ESA																		
Proton	1.00	0.25	1.07	1.00	1.00	1.13	0.87	0.93	0.80	0.80	1.07	1.07	1.20	1.07	1.07	1.07	1.07	1.07
Electron	1.00	0.25	1.06	1.02	1.02	1.11	0.87	0.91	0.83	0.83	1.09	1.09	1.17	1.06	1.09	1.09	1.09	1.09

**TABLE 11. Summary of Bias Voltage vs Energy Channel
Nominal Counts for Ion CEM.**

T9234-11

Energy Channel	i CEM Bias = 0	i CEM Bias = 1	i CEM Bias = 2	i CEM Bias = 3	i CEM Bias = 4	i CEM Bias = 5	i CEM Bias = 6	i CEM Bias = 7
0	64	78	83	77	95	107	110	125
1	56	66	79	71	88	95	120	135
2	69	62	86	89	95	91	125	132
3	63	72	69	86	86	111	108	119
4	65	63	77	86	77	112	101	117
5	59	62	66	80	79	96	105	130
6	56	66	73	83	74	83	97	101
7	59	62	69	68	77	87	99	105
8	42	55	60	64	78	75	84	106
9	44	47	53	57	63	67	79	89
10	36	39	43	42	57	54	76	75
11	31	34	43	43	45	49	62	56
12	17	18	26	23	34	31	41	37
13	10	14	22	13	24	17	23	28
14	7	7	9	8	6	6	10	12
15	3	4	3	4	2	4	6	5

**TABLE 12. Nominal Counts Normalized to Ion CEM
Bias = 0.**

T9234-12

Energy Channel	i CEM Bias = 0	i CEM Bias = 1	i CEM Bias = 2	i CEM Bias = 3	i CEM Bias = 4	i CEM Bias = 5	i CEM Bias = 6	i CEM Bias = 7
0	1.00	1.22	1.30	1.20	1.48	1.67	1.71	1.95
1	1.00	1.18	1.42	1.28	1.58	1.70	2.15	2.42
2	1.00	0.91	1.25	1.29	1.39	1.32	1.82	1.93
3	1.00	1.13	1.10	1.36	1.37	1.75	1.71	1.89
4	1.00	0.97	1.18	1.32	1.18	1.72	1.55	1.79
5	1.00	1.05	1.11	1.36	1.33	1.62	1.78	2.19
6	1.00	1.19	1.31	1.50	1.33	1.49	1.74	1.82
7	1.00	1.04	1.17	1.14	1.30	1.47	1.67	1.77
8	1.00	1.30	1.42	1.51	1.85	1.77	2.00	2.52
9	1.00	1.07	1.19	1.28	1.43	1.52	1.78	2.01
10	1.00	1.07	1.18	1.15	1.57	1.50	2.11	2.07
11	1.00	1.11	1.41	1.41	1.46	1.61	2.02	1.82
12	1.00	1.06	1.55	1.36	2.06	1.85	2.45	2.24
13	1.00	1.40	2.20	1.30	2.35	1.70	2.25	2.75
14	1.00	1.00	1.29	1.14	0.86	0.86	1.36	1.64
15	1.00	1.40	1.20	1.60	0.80	1.40	2.20	2.00
Sum 0 - 7	1.00	1.08	1.23	1.30	1.37	1.59	1.76	2.02

**TABLE 13. Summary of Bias Voltage vs Energy Channel
Nominal Counts for Electron CEM.**

T9234-13

Energy Channel	e CEM Bias = 0	e CEM Bias = 1	e CEM Bias = 2	e CEM Bias = 3	e CEM Bias = 4	e CEM Bias = 5	e CEM Bias = 6	e CEM Bias = 7
0	76	88	94	86	112	125	144	135
1	84	90	92	96	117	133	139	135
2	73	91	87	101	107	103	140	135
3	92	89	94	107	109	122	144	156
4	87	95	96	114	115	145	142	137
5	92	90	101	103	119	130	148	142
6	87	91	99	99	125	126	156	147
7	95	103	119	110	131	128	156	165
8	96	106	119	115	126	149	167	179
9	108	124	121	133	144	151	180	208
10	143	136	155	162	172	183	204	228
11	159	172	176	201	216	254	242	288
12	231	212	252	256	274	308	348	360
13	290	313	318	371	386	391	462	495
14	337	394	395	456	478	534	571	599
15	402	436	497	529	574	614	659	750

**TABLE 14. Nominal Counts Normalized to Electron CEM
Bias = 0.**

T9234.14

Energy Channel	e CEM Bias = 0	e CEM Bias = 1	e CEM Bias = 2	e CEM Bias = 3	e CEM Bias = 4	e CEM Bias = 5	e CEM Bias = 6	e CEM Bias = 7
0	1.00	1.16	1.25	1.13	1.48	1.66	1.91	1.78
1	1.00	1.08	1.10	1.15	1.40	1.59	1.66	1.61
2	1.00	1.25	1.19	1.39	1.48	1.41	1.93	1.86
3	1.00	0.96	1.02	1.16	1.18	1.33	1.56	1.70
4	1.00	1.09	1.10	1.30	1.32	1.66	1.63	1.57
5	1.00	0.97	1.10	1.12	1.29	1.41	1.61	1.54
6	1.00	1.05	1.14	1.14	1.45	1.46	1.80	1.69
7	1.00	1.08	1.25	1.15	1.38	1.35	1.64	1.73
8	1.00	1.11	1.25	1.20	1.31	1.55	1.75	1.87
9	1.00	1.15	1.12	1.23	1.34	1.40	1.67	1.93
10	1.00	0.95	1.08	1.13	1.20	1.28	1.43	1.59
11	1.00	1.08	1.11	1.26	1.36	1.60	1.53	1.82
12	1.00	0.92	1.09	1.11	1.19	1.34	1.51	1.56
13	1.00	1.08	1.09	1.28	1.33	1.35	1.59	1.71
14	1.00	1.17	1.17	1.35	1.42	1.58	1.69	1.78
15	1.00	1.08	1.24	1.32	1.43	1.53	1.64	1.87
Sum 10 - 15	1.00	1.06	1.15	1.26	1.34	1.46	1.59	1.74

are also listed in Table 14. These averages are approximately linear, with a slowly increasing slope as the bias level increases. These data represent operation within the plateau region of the CEM efficiency curve and below the noise region, which is the criterion for proper operation of the CEM.

The flight unit (S/N 001) drew between 1.15 and 1.49 W over the full range of input voltage, temperature, and operating conditions. It has a measured mass of 1.88 kg (4.15 lb).

SECTION 4

SURFACE POTENTIAL MONITORS

Two surface potential monitors (SPMs) are included as part of the FMDS to detect the charging of dielectric surfaces on the satellite. Because two different dielectric materials are to be used in flight, and because it is desirable to have them physically separated (to minimize their effect on each other), the best approach was to use two instruments, with the only difference being the dielectric material (see Figure 2).

4.1 BASIC SPM DESIGN

In designing the SPMs, one of the main requirements is that the charge buildup on the dielectric material is not altered because of the measurement. This dictates the use of some type of essentially infinite-impedance electric-field-sensing device.

Most electrostatic voltmeters with sufficient accuracy and resolution use a field-sensing probe that is closed-loop controlled to the same potential as the surface being measured. In this way, the field sensor only has to detect a null. To use this approach in this application, a "servo-amplifier" with an output of ± 20 kV would be required; this is not practical within the weight and power limitations for this instrument. We have chosen, therefore, to use the approach adopted by the NASAs Lewis Research Center for their surface-voltage sensor (SVS).² The NASA approach retains most of the advantages of a feedback sensing system, yet does not require high voltage. This system uses a combination of electrodes that attenuates the field produced by the sensing surface, and allows it to be nulled with a low-voltage ($< \pm 10$ -V) feedback signal (see Ref. 1 for details).

4.2 SPM DESIGN CONSIDERATIONS

The flight design of the SPM at the time of the critical design review is shown in Figure 8, where the input electrode is supported by an annular insulating ring. This allows the dielectric sample to extend past the input electrode onto the annular insulating ring, thereby shielding the electrode from any particles or plasma in the immediate vicinity. The input electrode with the dielectric material on its surface is insulated from the rest of the instrument by the annular insulating ring. The electrostatic voltmeter measures the potential of the input electrode; however, no direct electrical connection is made to it. The potential of the front surface of the dielectric is transferred to the input electrode by capacitive coupling. Therefore, if the input electrode is to closely track the dielectric front surface, the capacitance from the input electrode to ground must be much smaller than the capacitance between the dielectric front surface and the input electrode.

A possible problem with the SPM is the input electrode gathering some charge not related to the potential of the dielectric front surface. This charge would then introduce a zero offset into the SPM. The breadboard design called for a shorting relay and software routine that would connect the input electrode to ground when the SPM was in full sunlight. Under full sunlight conditions, the dielectric front surface should be within 100 V of ground, and therefore, the SPM would be zeroed to within 100 V. This scheme required that the spacecraft periodically rotate the SPMs into full sunlight. This requirement and the need for a small, lightweight 20-kV relay turned out to be significant engineering problems.

The flight design calls for deleting the relay and using a 2-h time constant (RC network) to discharge the input electrode. A 2-h time constant requires approximately $10^{13} \Omega$ from the input electrode to ground; this could conceivably be provided by the

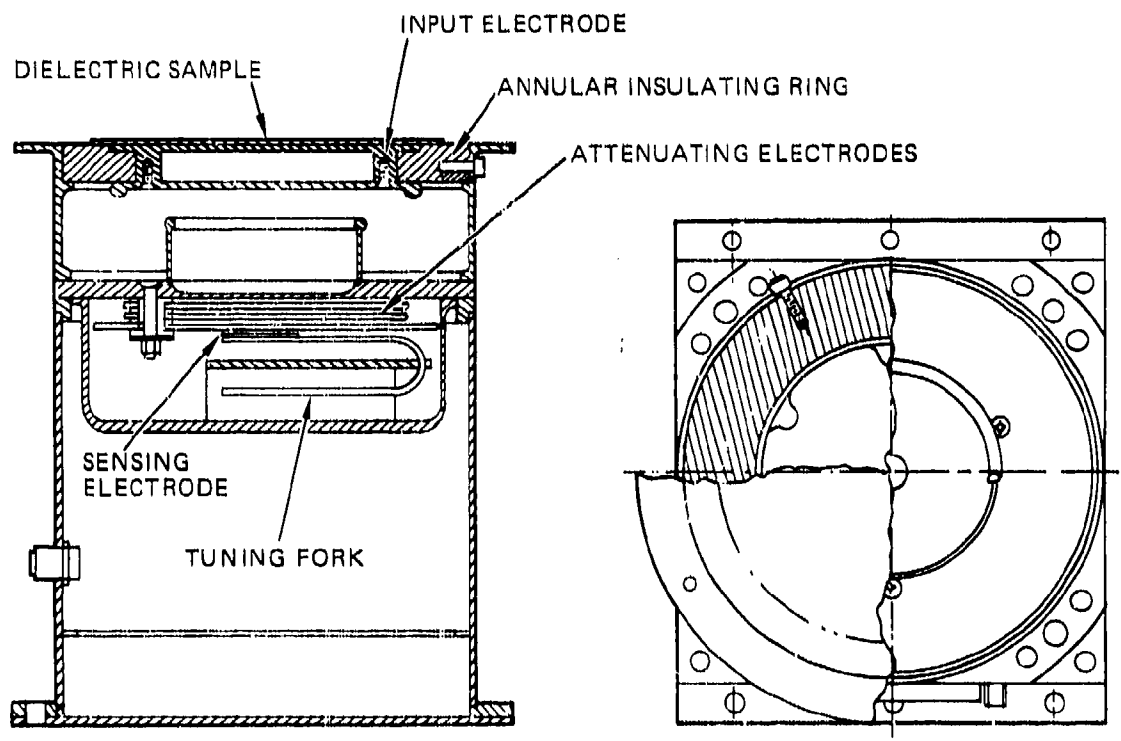


Figure 8. Flight package design for the SPM.

leakage of the annular insulating ring. A normal operating scenario has differential charging, which would immediately charge the front surface of the dielectric, and the input electrode would go to the same potential. The 2-h time constant will start to bleed the charge from the input electrode; however, differential charging normally occurs in minutes, and if it is of any significant level, the plasma source will be turned ON. The plasma source will immediately remove the charge from the front surface of the dielectric and return it to ground. The 2-h time constant will then reset the input electrode to ground. The problem with this approach is that very slow (compared to 2-h) differential charging will not be detected by the SPMs.

We tried using Vespel for the annular insulating ring, and tested it in a vacuum chamber under simulated operating conditions. Vespel demonstrated an acceptable initial time constant; however, the input electrode decayed toward a voltage level that was in the range of 25 to 90% of the voltage originally applied to the input electrode - the level depending on the length of time the voltage was applied before allowing the input electrode to start decaying. The input electrode appeared to decay with a much longer time constant (> factor of 10) after the initial time constant. Fused silica and G-10 glass epoxy exhibited characteristics similar to Vespel.

These decay characteristics are not fully understood; however, we believe that the characteristics observed are due to charge migration both on the surface and in the bulk of the insulating ring. Furthermore, the resistance provided by the insulating ring is too high, by at least an order of magnitude, to provide a 2-h RC time constant. Therefore, we have added a discrete resistor between the input electrode and ground (Figure 9) to swamp out the undesirable characteristics of the insulating ring material and to provide the proper RC time constant.



Figure 9. SPM input electrode assembly showing the discrete resistor (5 resistors in series) between the input electrode and ground (flying lead).

Figure 10 shows the RC time constant of the input electrode under conditions simulating the SPM being in the sun. The simulation consists of the SPM being in a vacuum chamber with UV light shining on the dielectric sample (VDA-backed 2-mil Kapton), with a $2.7 \times 10^{13} \Omega$ resistor from the input electrode to ground. While this resistance value is low enough to eliminate the zero-offset problems, figure 10 shows a time constant of approximately 12 h, which is a factor of 6 too long. A proper value resistor was not available at the time of the test to provide the required 2-h time constant.

4.8 SPM FLIGHT HARDWARE

The 12 circuit boards for 4 SPMs have been assembled. The interconnect wiring for two units has been completed and one unit has been assembled. During assembly we discovered that the tuning fork was too close to the compensating electrodes. This was corrected by fabricating a 0.200-in.-thick spacer to provide the proper spacing. A shield was also added to the design to isolate the 90-V peak-to-peak drive signal for the tuning fork from the very sensitive sensing electrode for the electronics. Figure 11 is a photograph of the complete SPM.

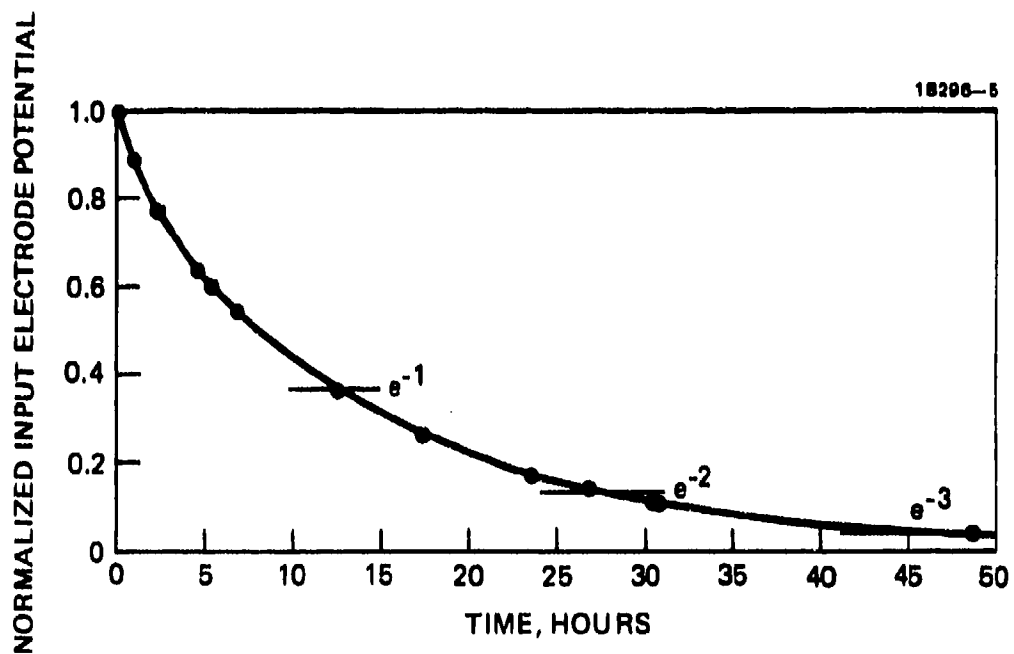


Figure 10. SPM input electrode time response under simulated sunlight conditions.

MC17992

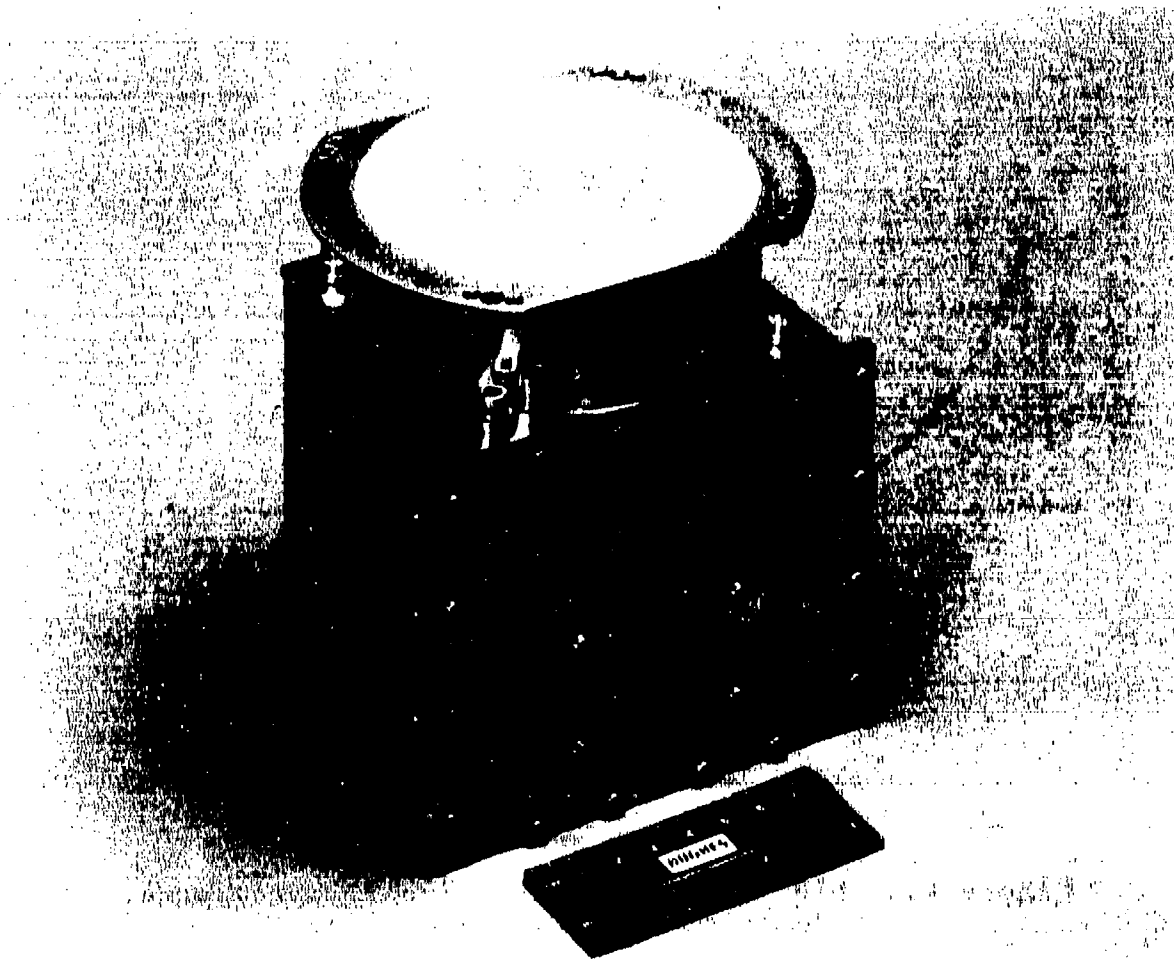


Figure 11. A complete SPM.

SECTION 5

TRANSIENT PULSE MONITOR

The Transient Pulse Monitor (TPM) is included as part of the FMDS to detect the onset of arcing on spacecraft surfaces. The main requirement in the selection of the TPM sensor design is maximized ability to discriminate between signals generated by arcing events, and signals caused by "legitimate" spacecraft circuit transients. A secondary consideration is the need to register arcs occurring anywhere on the spacecraft surface with a minimum number of sensing elements.

A review of the literature revealed that the main types of effects caused by arcing on a spacecraft are those in which:

- (1) The arc causes "blow-off" of a cloud of electrons that rapidly disperses. This geometrical change causes a pulse of electrostatic field, which can be detected by capacitive coupling to an electrometer plate. This electrostatic field can be detected, weakly perhaps, beyond the line of sight.
- (2) The arc creates a plasma that radiates at high frequency. This in turn causes a pulse of wideband rf energy to appear, with its source in the plasma cloud and randomly polarized. This energy can be detected by antennas (horns, dipoles, monopoles, etc.); for the most part, the radiation can be sensed in line of sight only.
- (3) During the pre-arc stage, an increasing electrostatic potential appears (probably at the surface of dielectric materials). The arc causes a substantial collapse of this potential, which can be detected by capacitive coupling to an electrometer plate. The width of the detected pulse is determined by the low frequency response of the detection equipment, rather than any characteristic of the arc signature itself. The collapse of the potential can be detected beyond the line of sight.
- (4) The arc causes replacement currents, which can be detected by current sensors, to flow in the conducting skin of the satellite.

Effect (4) has been employed on several satellites (e.g., SCATHA and the Canadian Technology Satellite) as a means of detecting arcs. The major problem encountered with this technique is its inability to differentiate between arcs and legitimate spacecraft transients, particularly in real-time. Therefore, it was not seriously considered for this application.

The remaining effects can be classified by the type of detector required. Effects (1) and (3) utilize an electrometer plate (E-field antenna), which is broadband, while effect (2) requires an rf antenna, which is narrowband. The relative merits of these two detection methods follow:

- If only a single detector with a single antenna outside the Faraday cage of the spacecraft is used, the ability to discriminate correctly between arcs and transients appears equally limited for both detection methods.
- A single broadband antenna is more likely than a single rf antenna to pick up a detectable signal from an arcing event occurring at a location far below the horizon of the antenna (i.e., far from having a line-of-sight connection with it).
- Regardless of the detection method, the addition of a second antenna inside the spacecraft Faraday cage, in conjunction with a simple pulse-analysis circuit, offers a much increased probability of correct discrimination between arcs and transients by permitting a comparison of signals received inside and outside the Faraday cage.
- It is more likely that the signals received by two broadband antennas, rather than by two rf antennas, will have amplitude ratios that will characterize arcs and transients properly, irrespective of the location of the event relative to the antennas.
- Additional practical points in favor of the broadband approach are ease of protection from destructive overloads caused by arcs adjacent to the antenna, and lower power consumption.

The TPM design for the FMDS is based on the broadband detection approach, utilizing a 123-cm² E-field antenna outside the spacecraft Faraday cage and connected to a 250-Hz to 75-MHz broadband amplifier and pulse analysis circuitry, and a second 123-cm² E-field antenna with greatly simplified pulse analysis capabilities inside the Faraday cage. The detailed design is discussed in Scientific Report No. 2.¹

Testing of the TPM electronics has revealed that the highest sensitivity of the TPM is lower than expected (and specified) (i.e., approximately 200 instead of 10 V/m). This reduced sensitivity is mainly due to higher capacitance to ground in the flight design of the antenna plate and front-end electronics circuitry. It will be corrected by increasing the spacing between the antenna plate and ground, bootstrapping the ground plane under the front-end electronics circuitry (Figure 12), and modifying the peak detection circuitry to be more sensitive to narrow, low-amplitude pulses. Figure 13 is a photograph of a flight TPM antenna assembly.

M17722

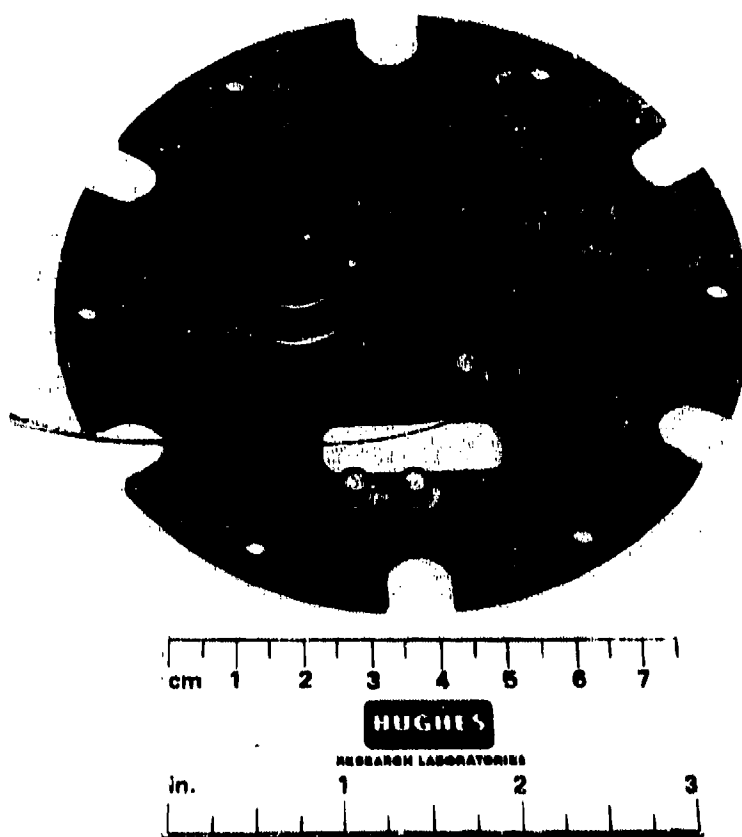


Figure 12. A TPM input buffer circuit board.

MC17095

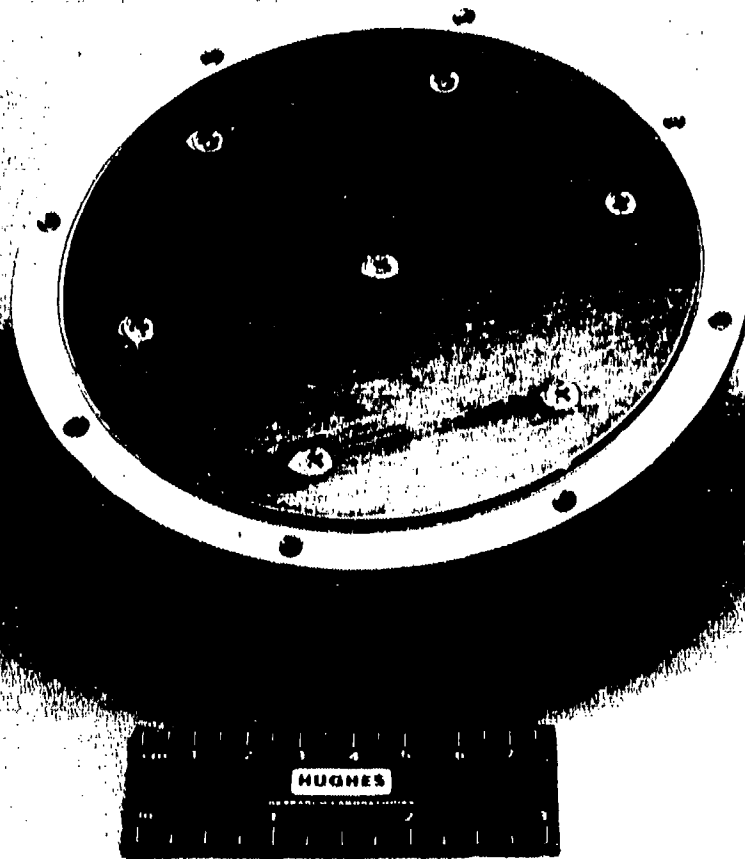


Figure 13. A flight TPM antenna assembly.

This Page Intentionally Left Blank

SECTION 6

CONTROLLER

The controller provides autonomous control of the FMDS relative to the remainder of the satellite, and also ties together the other units of the FMDS. The "brain" of the controller is a microprocessor that contains the algorithms necessary to interpret the data from the sensors and to command the plasma source to turn ON when spacecraft charging is occurring. It then monitors and maintains the stability of the operation of the plasma source. The controller turns the plasma source OFF after a programmable time-out, when the emission current from the plasma source has been less than a threshold value for a specified period of time, and/or the ambient electron environment returns to a quiescent condition. The controller has the ability to accommodate certain instrumental faults and failures and to adjust instrument parameters. It is also the command and telemetry interface with the satellite.

The five circuit boards and the backplane for one flight controller electronics box have been completed (except for some install-after-test components and conformal coating). The controller I/O board is shown in Figure 14, and an analog-to-digital converter (ADC) and I/O board in Figure 15. The controller electronics box with the five circuit boards installed, but without the box end-plate, is shown in Figure 16.

The master microprocessor, CMD/TLM and I/O, controller I/O, and ADC and I/O boards have all been tested for functionality and are operational. Only the ESA Microprocessor board has not yet been checked out. The ADC was tested and calibrated at the board level and performs better than the breadboard. The calibration curve is shown in Figure 17 and includes the multiplexer and the sample/hold amplifier as part of the calibration.

M17721

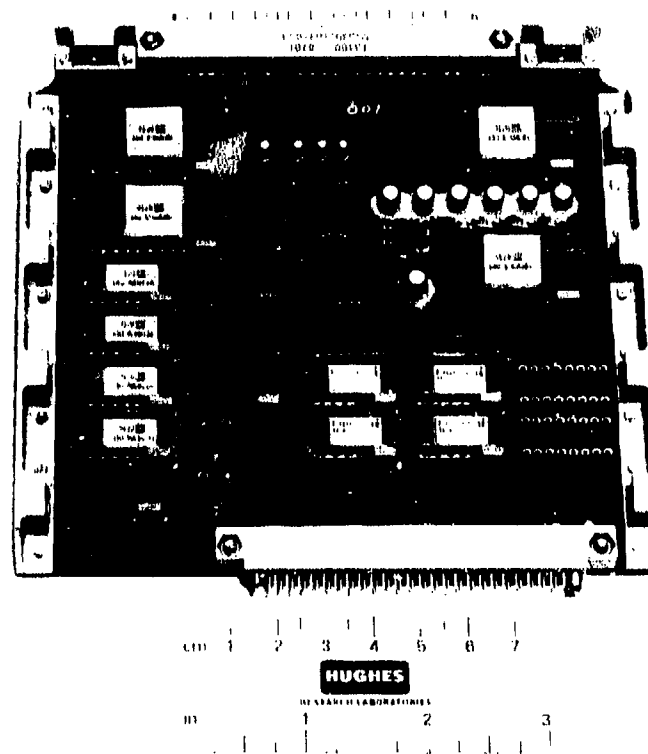


Figure 14. Controller I/O board, S/N 001.

M17720

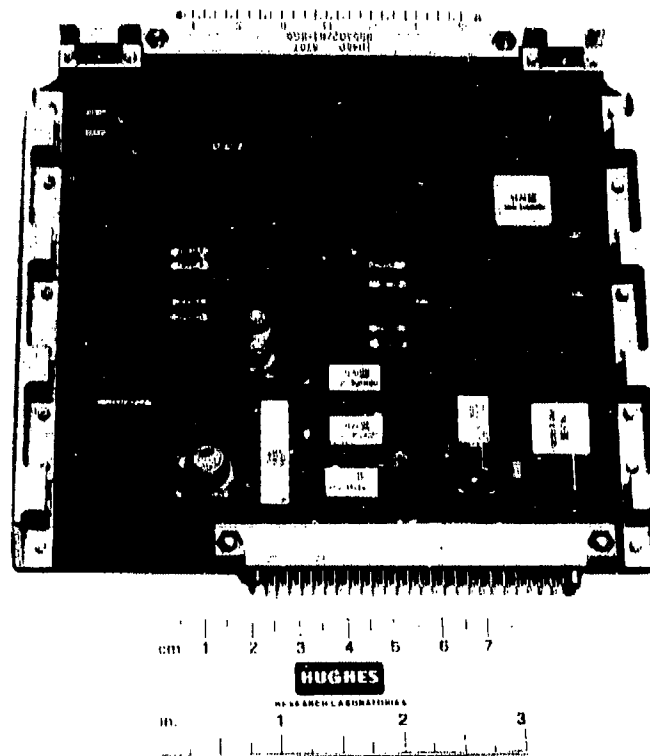


Figure 15. ADC and I/O board, S/N 001.

MC17993

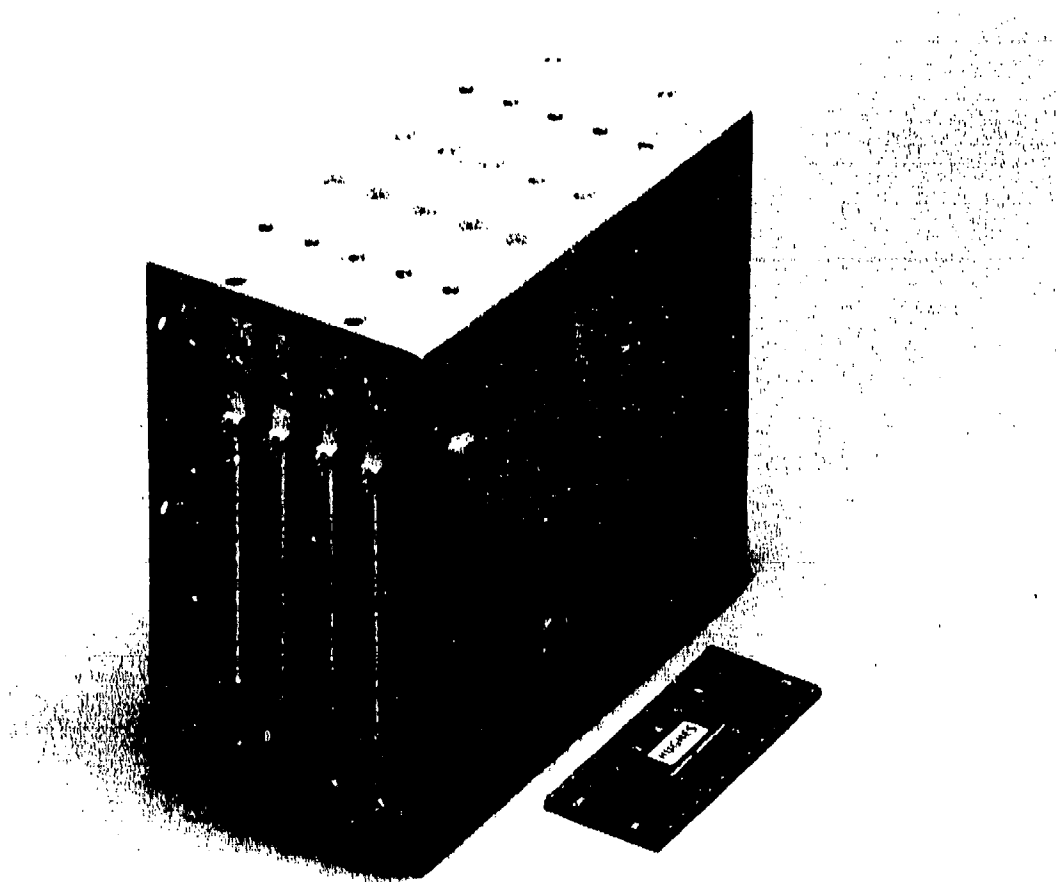


Figure 16. Controller electronics box without the box end-plate.

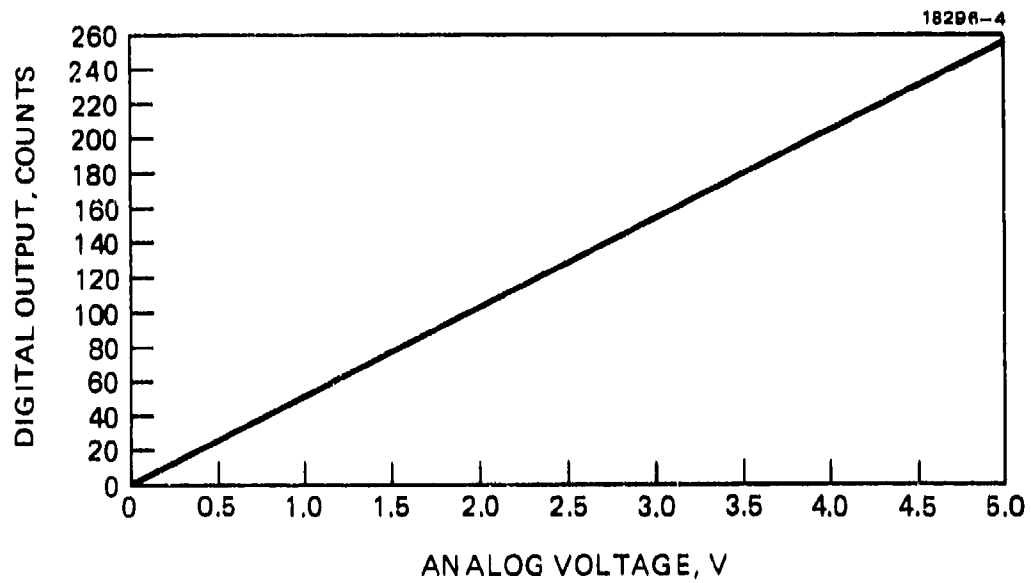


Figure 17. Calibration of the ADC on ADC and I/O board S/N 001.

All the software modifications that resulted from the critical design review have been written for the master microprocessor but have not yet been tested. The software grew from 10,078 to 11,082 bytes as a result of these modifications. A total of 16K bytes of memory is available in the master microprocessor.

SECTION 7

PLASMA SOURCE

The FMDS plasma source consists of three subsystems: the plasma generator, the power electronics required to operate and control the plasma generator, and the expellant storage and control assembly. The plasma generator has been developed to breadboard level under a Hughes IR&D project, and this technology has been provided to the FMDS program for the flight plasma generator design.

7.1 PLASMA GENERATOR DESIGN

The plasma generator is regarded as the major element of the system, because its design and operating characteristics determine the requirements for the other two elements (power supplies and feed system). The plasma generator has the general characteristics shown in Table 15.

The plasma generator (Figure 18) is a compact arrangement of a hollow cathode, keeper and anode electrodes, a magnetic structure, and a ground shield. Xenon gas flowing through the plasma generator is ionized by bombardment with electrons released from a low-work-function surface within the hollow cathode. The ionized gas flows out of the plasma generator, providing a medium density ($\sim 10^{10}/\text{cm}^3$), inert-gas plasma to neutralize differential charge buildup between various surfaces of the spacecraft, and also to form an electrically conducting "bridge" between the spacecraft and the natural space plasma.

A <1 -s plasma generator turn-ON time is achieved by gas-burst ignition. Approximately 1000 V is applied between the keeper and the cathode, and then a burst of high-pressure gas (few hundred torr) is admitted to the cathode. The keeper voltage falls almost immediately (<1 ms) to <20 V. We believe that the ignition process consists of the formation of an arc that runs on a small spot on the insert until the insert temperature is raised to the point of thermionic emission. At

TABLE 15. SPACECLAMP Plasma Generator Characteristics.

T9234.15

Parameter	Value	Unit
Expellant flow rate	<40	mA Equiv
Discharge voltage	<40	V
Discharge current	<250	mA
Keeper voltage	<25	V
Keeper current	<400	mA
Total power (run)	<10	W
Total power (conditioning)	20	W
Ignition time	<1	S
Expected lifetime	>1200	Hours
Expected restart capability	>1000	Starts
Ion-emission current (max)	>1	mA

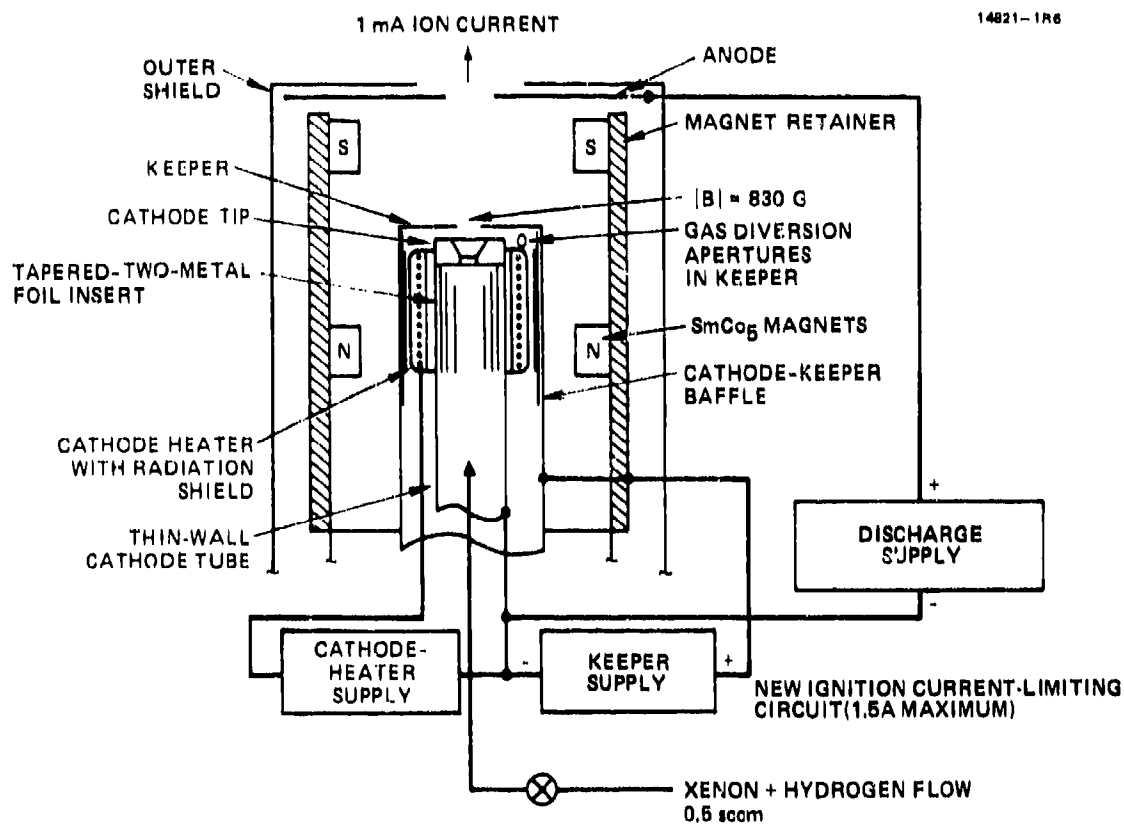


Figure 18. Simple schematic of the plasma generator.

this point, cathode operation undergoes a rapid transition to a low voltage hollow-cathode mode. The total energy input during the high voltage portion of the ignition transient is about 0.25 J, which is nondestructive to the insert. The gas pressure and flow settle out to the nominal 0.5 sccm condition after approximately 120 s.

The rolled-foil insert consists of 0.013-mm (0.5-mil)-thick rhenium foil with a sputter-deposited linear platinum grid deposited on one side. A Hughes proprietary emissive mix is sprayed on both sides of the foil to provide a low work function medium for electron emission. The rhenium foil is then rolled into a cylindrical structure for insertion into the cathode.

The flight design of the plasma generator is shown in Figure 19, and an exploded view of a flight source in Figure 20. The plasma generator is designed as a hermetically sealed unit so that it can be evacuated (through a remove-before-launch cap) and operated during ground testing and spacecraft integration. The cathode, keeper, and anode are all electrically isolated from the outer shell so the return current from the spacecraft can be measured.

7.2 TEST RESULTS

One of the flight plasma sources has undergone testing. This source (S/N 003) is the first of three to be fabricated and assembled. S/N 003 is not planned to be flown, but is identical to S/N 001 and S/N 002, which are planned to be the flight sources.

S/N 003 was tested to verify the flight design that was structurally modified from the breadboard source in a manner not expected to significantly affect operating characteristics. However, the first operation of S/N 003 was very erratic and unacceptable, as shown in the stripchart recording of Figure 21. The keeper voltage continuously drifted, jumped around, and never stabilized. In addition, both the keeper and discharge

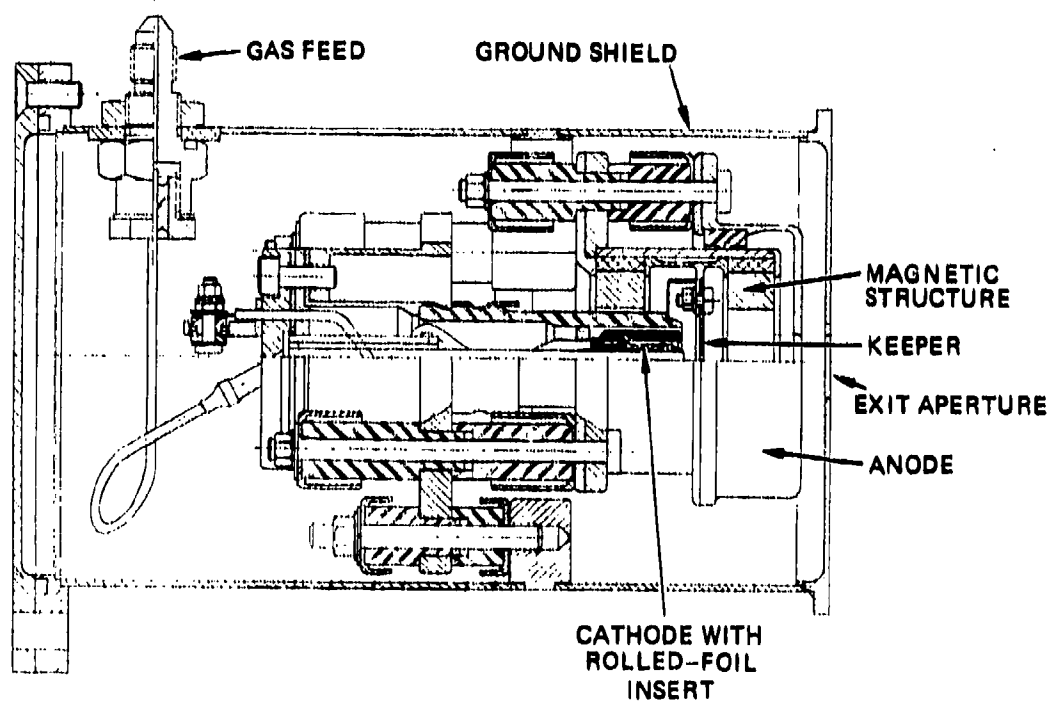


Figure 19. Cross section of the flight plasma generator.

MC17489

17168-1

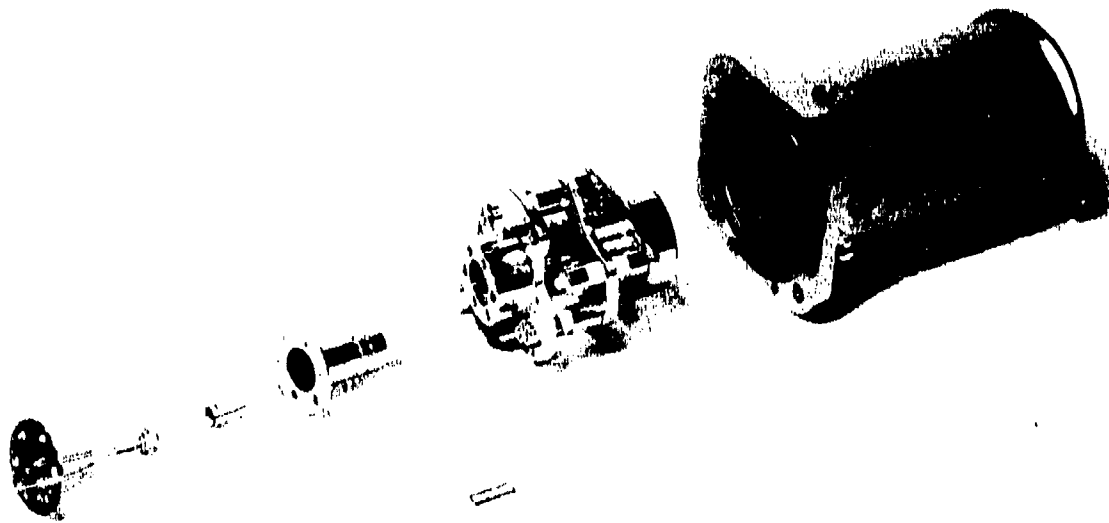


Figure 20. A flight plasma generator in an exploded configuration.

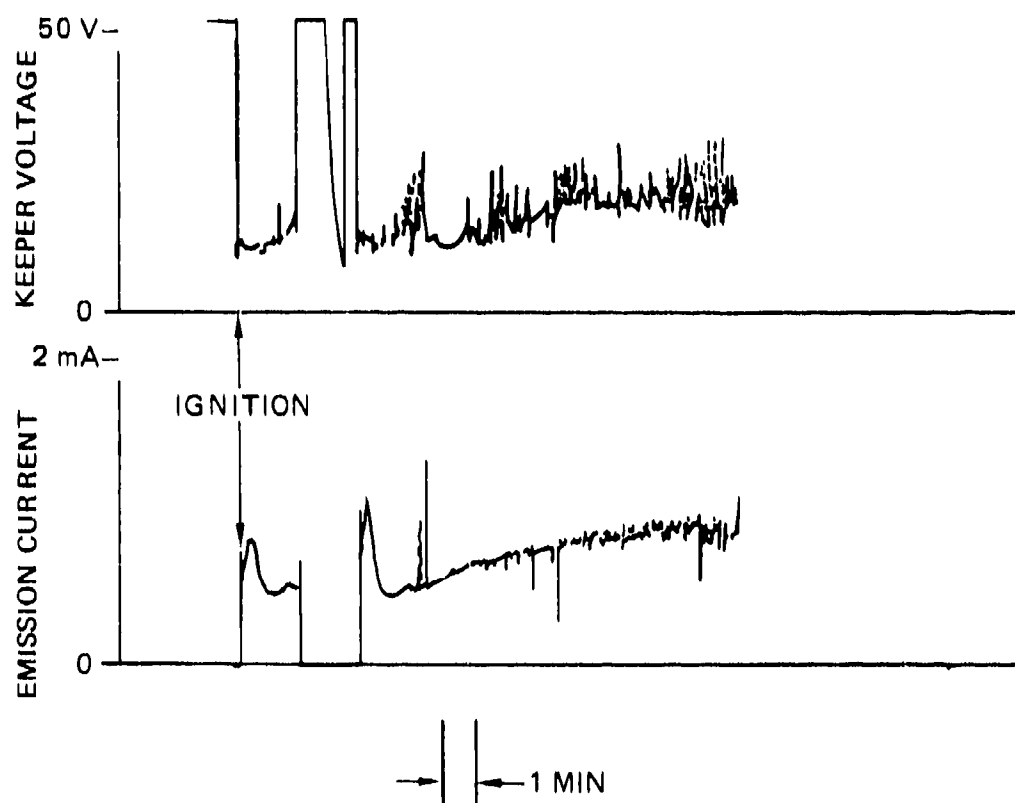


Figure 21. Stripchart recording of the keeper voltage of source S/N 008 during initial and unacceptable operation (contaminated cathode and insert).

voltages were higher than expected. This type of operation was thought to be indicative of contamination of the cathode and its insert; however, a problem with the design was still a possibility at that time.

We were in the process of replacing the cathode insert with one we knew was good (from the breadboard source), when we discovered that some of the components in the source were very discolored and abnormal looking. We had these parts analyzed and concluded that an air leak in the feed system, which was later discovered, had contaminated the source, as evidenced by the copper and rhenium oxides present. We also concluded that a dark material on the heater-lead outer conductor and the mounting collar was stainless steel that was vapor deposited on those components during fabrication. When the heater lead was brazed into the mounting collar, the brazing fixture had stainless steel screws, which disappeared during the brazing operation. These parts were grit blasted in an attempt to remove the stainless steel; however, the presence of some stainless steel in these areas is not considered to be a problem.

All parts of the source were cleaned, a new cathode insert was installed, and the source was reassembled. As an additional guard against contamination, we cleaned the vacuum chamber in which the source was tested. Figure 22 shows a stripchart recording of the keeper voltage during subsequent testing. It is very stable and well-behaved (after the normal ignition transients), and the keeper and discharge voltage levels are very acceptable.

Ion emission current (I_E) as a function of keeper current (I_K) and discharge current (I_D) is shown in Figure 23. The two operating points depicted in this figure and Figures 24 and 25 are detailed in Table 16. We can see from Figure 23 that higher I_E (than our nominal of approximately 1 mA at $I_K = 250$ mA and $I_D = 200$ mA) can be obtained by going to a lower keeper current

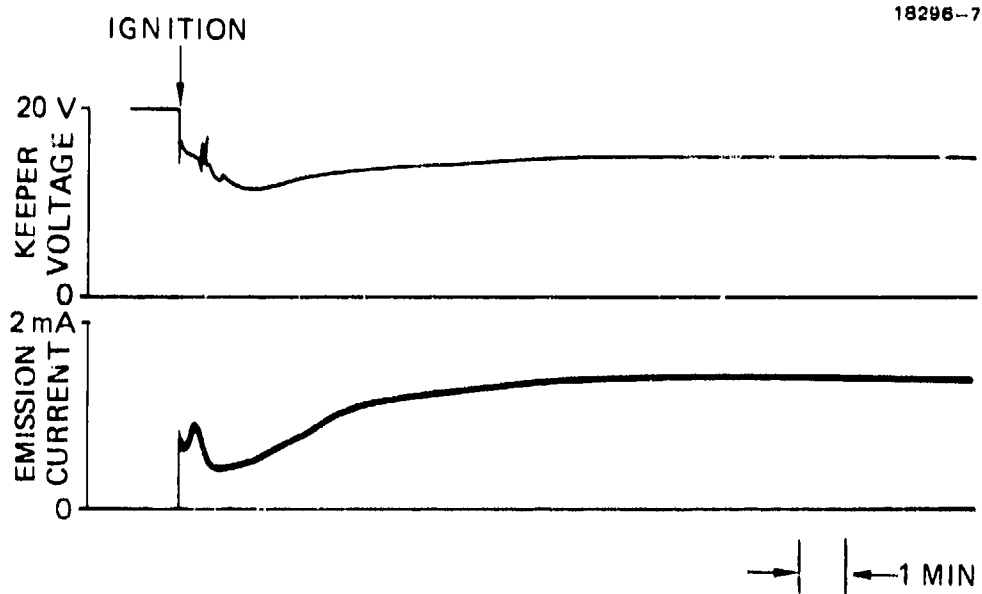


Figure 22. Stripchart recording of the keeper voltage of source S/N 008 after elimination of the contamination problems, showing very good performance.

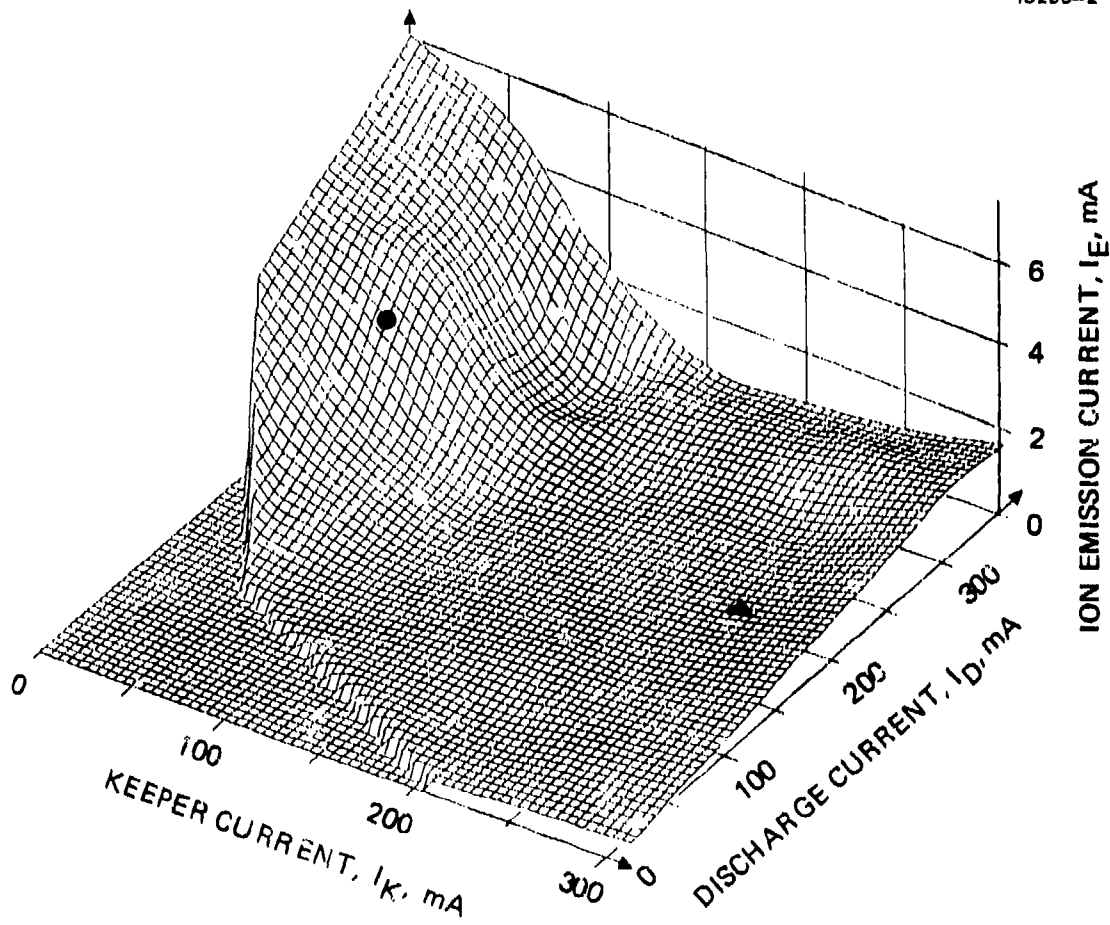


Figure 23. Ion emission current as a function of keeper current and discharge current.

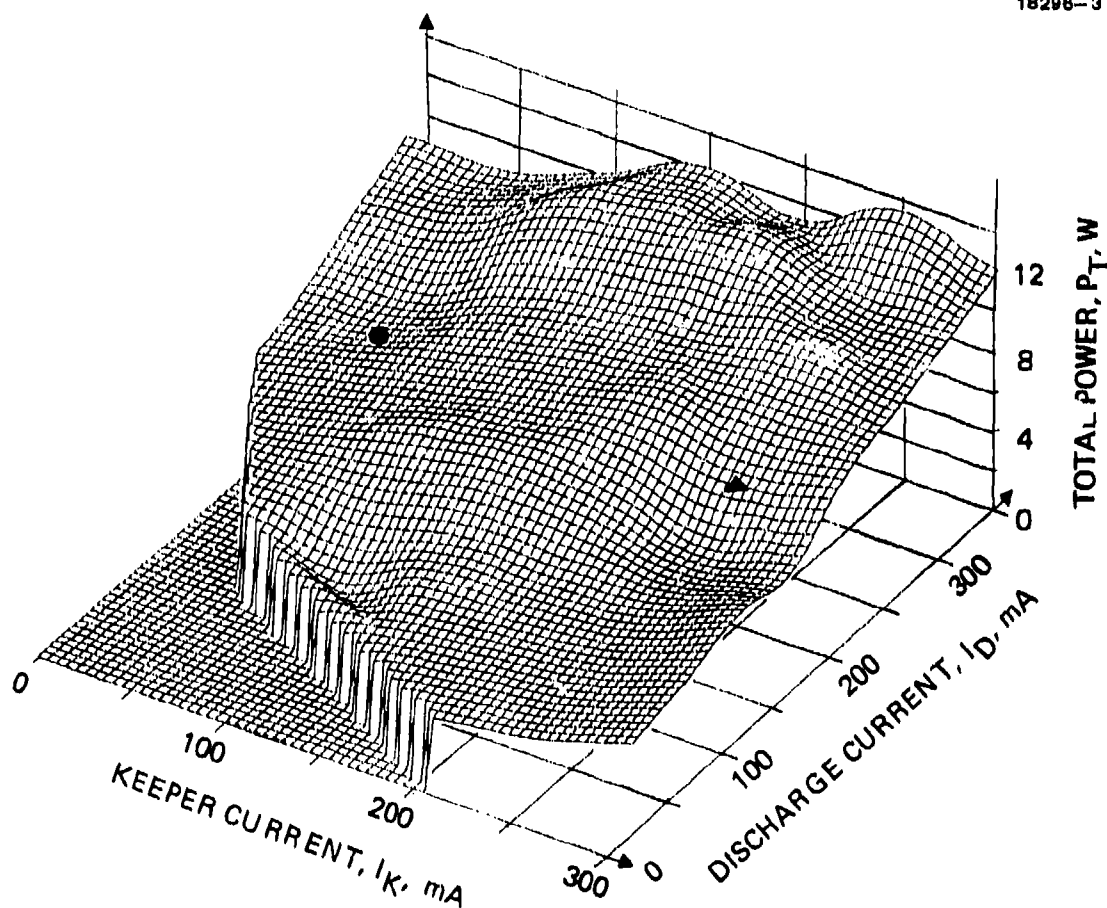


Figure 24. Total input power to the source as a function of keeper current and discharge current.

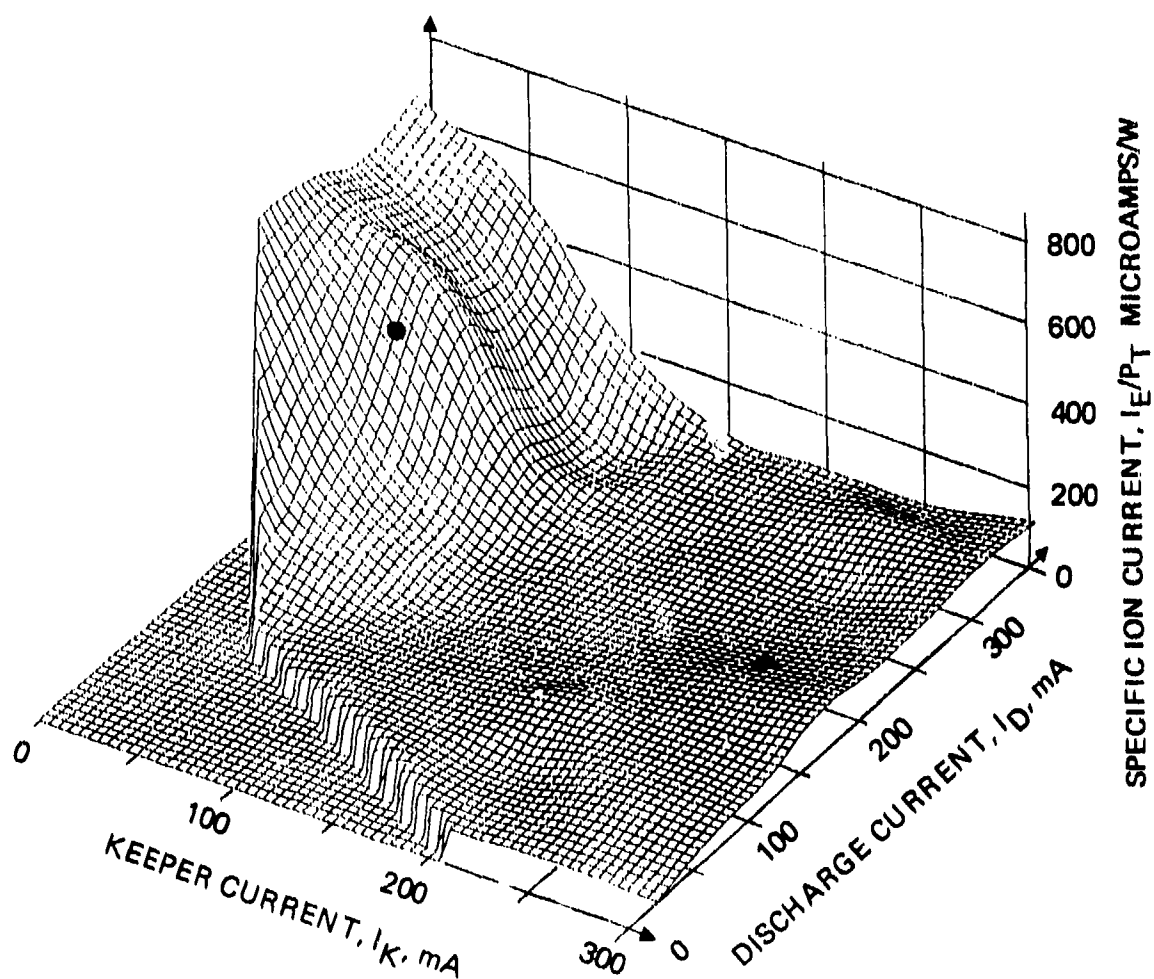


Figure 25. Specific ion emission current ($\mu\text{A/W}$) as a function of keeper current and discharge current.

TABLE 18. Operating Points Illustrated in Figures.

T9234-16

Point:	●	▲
Keeper:	11.4 V, 50 mA	13.9 V, 250 mA
Discharge:	23.4 V, 250 mA	23.7 V, 200 mA
Ion emission:	3.49 mA	0.967 mA
Gas flowrate:	0.46 sccm	0.46 sccm
Total power:	6.42 W	8.22 W

and a slightly higher discharge current ($I_E = 3.5$ mA at $I_K = 50$ mA and $I_D = 250$ mA). Figure 24 shows total input power to the source as a function of I_K and I_D . It is interesting to note that the higher I_E region from Figure 23 actually requires less power than our nominal point. Specific ion emission current in $\mu\text{A/W}$ is plotted against I_K and I_D in Figure 25. This figure shows that the source performance is definitely much better at lower keeper currents.

Based on the data cited above, we recommend that one of the alternative source operating points be in the vicinity of $I_K = 50$ mA and $I_D = 250$ mA, where I_E is approximately 3.5 mA. It should be noted, however, that it is necessary to start the source at the nominal operating point and then switch to the lower I_K point after the ignition transient is complete (1 to 2 min).

Testing of the first plasma source electronics unit has begun. All power supplies and associated circuitry are operational, with some minor problems that need to be evaluated and corrected. The optical isolators that isolate the drive circuitry from the power circuitry for the discharge, keeper, and heater supplies are introducing noise into these circuits. This will be corrected by grounding the P.C. board foil under the optical isolator and the lid of the optical isolator package. The drive circuit for the power and valve inverter (provides power to operate the feed system valves and the relays that turn the sensors ON/OFF) does not provide sufficient dead band, causing the power transistors to both be ON momentarily, which results in large current spikes and excessive power draw on the input power bus. This problem is being evaluated. A photograph of the plasma generator electronics board No. 2 is shown in Figure 26.

M17719

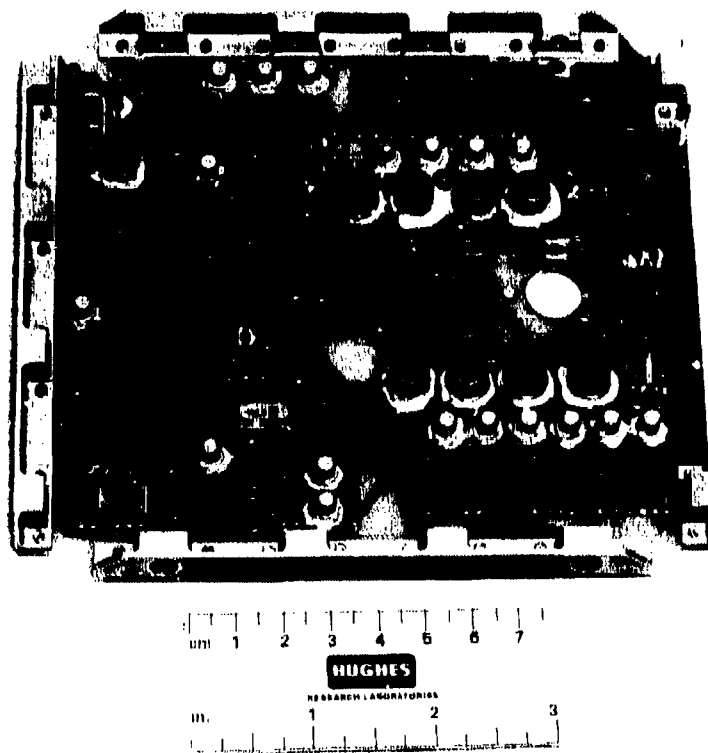


Figure 26. Plasma growth electronics board no. 2,
S/N 001.

7.3 CONTAMINATION MEASUREMENTS

The possibility of contaminants emanating from a plasma generator is always a concern to spacecraft designers, especially where optical and thermal control surfaces are involved. Therefore, during the lifetest of the breadboard plasma generator, we installed three glass "witness" slides within the vacuum chamber to measure the deposition of any contaminating substances that might emanate from the plasma generator.

The slides were placed in the positions shown in Figure 27. Slide #3 was directly below the exit aperture of the plasma generator and slide #4 was approximately 17 cm further downstream. Both slides were mounted on a perforated steel mesh vacuum-chamber liner (diameter = 23.4 cm). Slides #1 and #2 were control slides, with #2 placed within the vacuum chamber but upstream of the plasma generator and isolated from the emitted plasma by a perforated mesh. Slide #1 was never placed in the vacuum chamber.

After the lifetest, we found that slide #3 had become coated with a brownish material, while slides #2 and #4 still appeared clear. Light transmission analysis of all four slides indicated that slides #1, #2, and #4 had similar characteristics, while slide #3 showed transmission loss compared with the other three. This transmission loss as a function of wavelength is shown in Figure 28. We used electron spectroscopy for chemical analysis (ESCA) to measure the relative amounts of any surface-deposited elements on slides #1, #3, and #4. No contaminants were identified on slides #1 and #4, while slide #3 was found to have carbon and sodium. We believe this contamination is due to vacuum-pump oil that backstreamed onto the slide and subsequently decomposed under bombardment by plasma ions and electrons.

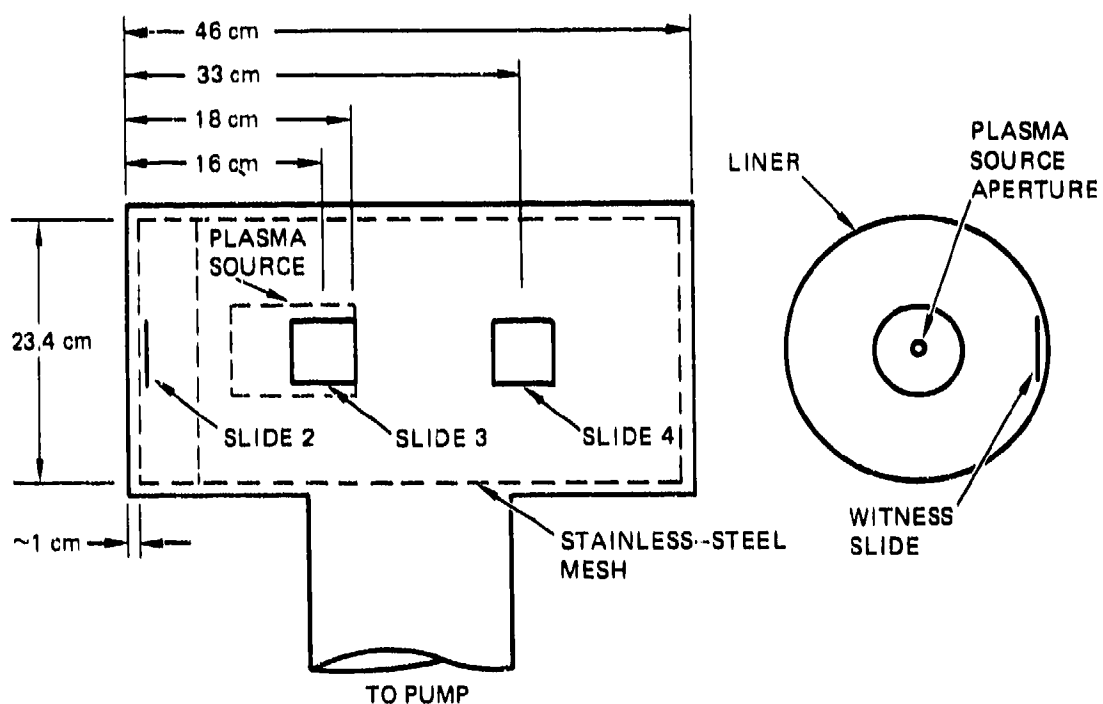


Figure 27. Positions of the contamination "witness" slides during the plasma generator lifetest.

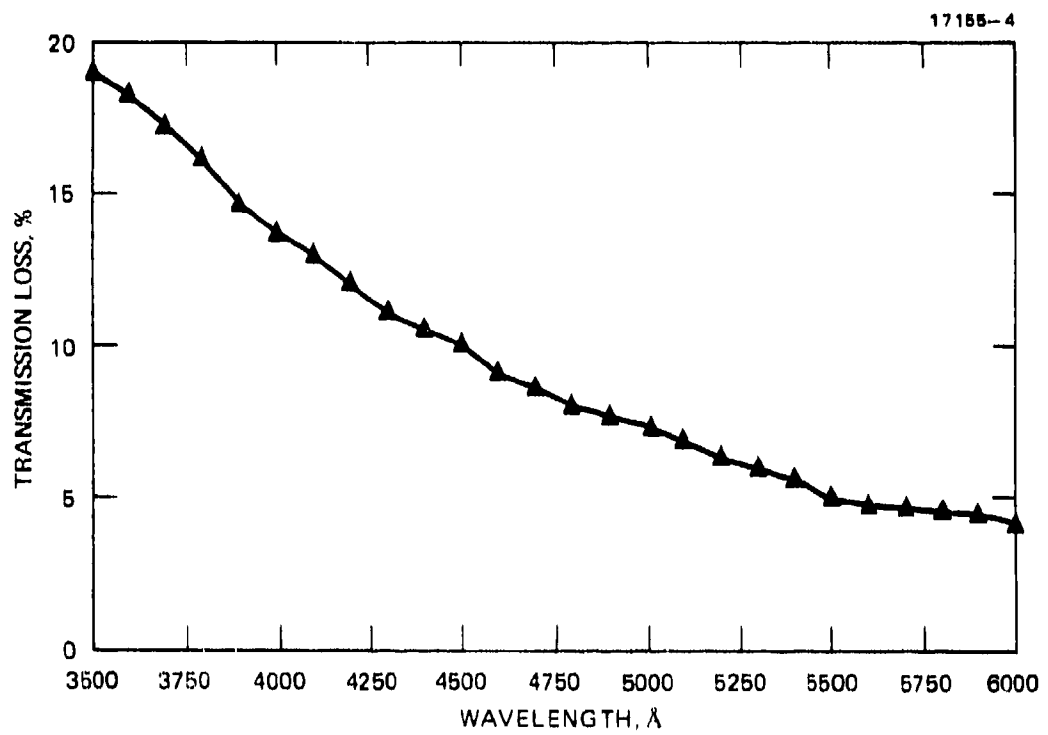


Figure 28. Optical transmission loss of contamination "witness" slide 3.

Contaminants that might be emitted from the plasma generator are barium, strontium, calcium, platinum, rhenium, molybdenum, iron, samarium, cobalt, stainless-steel, tantalum, and tungsten. None of these were found on the witness slides.

We also used optical spectroscopy to determine if there were sputtered-metal contaminants present in the efflux of the FMDS plasma source during operation. These contaminants, if present, would pose a potential deposition hazard to nearby sensitive spacecraft surfaces. While we do not expect sputtering within the FMDS plasma source (because the voltages present in the source are generally below the sputtering threshold for the materials that compose the discharge chamber), we have had only limited experimental confirmation of this expectation. In the present work, we found no contaminant spectra in the FMDS plasma source optical emissions. This finding is in agreement with the above results for the glass "witness" slides, giving us a high level of confidence that the FMDS plasma source efflux is free of contaminants.

Figure 29 shows the simple apparatus we used for the measurements. Light from the FMDS plasma source Penning-discharge plasma is imaged onto the slit of a 0.25-m Jarrell-Ash monochromator, which is equipped with a stepping-motor grating drive. As the grating moves, spectral lines fall on the exit slit, where they are detected by an R212A photomultiplier tube. The photomultiplier output is recorded on a stripchart recorder. We calibrated the system by placing commercial neon and krypton calibration lamps at the location of the plasma source and recording their spectra. By using these known spectra as guides, we could determine the wavelengths of lines emitted by the FMDS plasma source with a high degree of accuracy.

To determine if contaminants were present, we compared the observed spectrum with published atomic and ionic persistent-line spectra for xenon and hydrogen and for the candidate contaminants iron, tungsten, molybdenum, tantalum, platinum, and

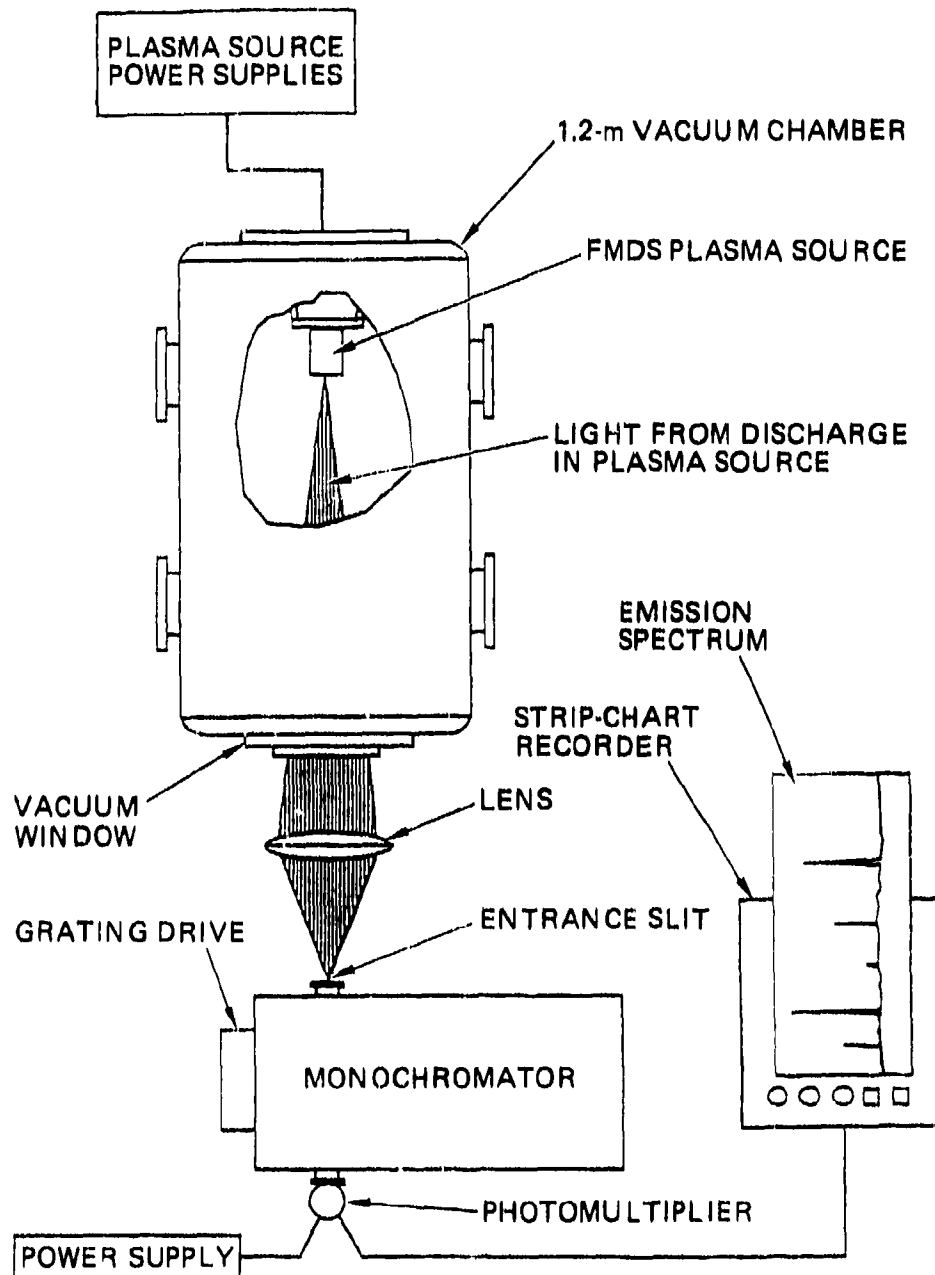


Figure 29. Apparatus used in FMDS spectroscopic measurements.

rhenum. Generally, if a given species is present in a Penning discharge, it will be represented by multiple spectral lines, because electrons in the discharge are sufficiently energetic to excite a large number of atomic energy levels. In some cases individual spectral lines of the candidate contaminants can coincide with those of xenon or hydrogen lines (within the resolution of our instrument), making unambiguous identification of those particular lines impossible. For tentative species identification, we require the presence of at least one unambiguous spectral line; positive identification requires multiple unambiguous lines. Using this criterion, we found no evidence (tentative or otherwise) of any of the candidate contaminants. Each of the candidate contaminants has strong persistent lines that fall into regions of the spectra that would make them clearly distinguishable from xenon and hydrogen lines; none of these lines were detected.

The occurrence of a null result, as obtained above, always brings with it the question of whether the apparatus was sufficiently sensitive. While more sensitive measuring techniques (photon counting, laser fluorescence, etc.) certainly exist, we have previously used the same spectroscopic apparatus to detect contaminants in the emissions spectra of ion-thruster Penning discharges, which run at a slightly higher discharge voltage. In these measurements, we easily detected iron and molybdenum spectral lines when voltages within the ion thruster were above the sputtering threshold. These previous results lend credence to our ability to detect contaminant atoms at levels that (for the ion-thruster application) have been judged not hazardous to the spacecraft.

Another possible concern to a spacecraft is condensation of xenon expellant on cryo-temperature surfaces. Neutral xenon gas released from the plasma generator will condense and freeze (xenon has a 161K freezing point) on cold (100K) optical surfaces, potentially forming a thin xenon-ice coating that

could degrade the optical properties of the cold optical elements. We present very simple calculations below that indicate that no buildup of condensing xenon will occur at the 100K optical-surface temperature, and that only a small fraction of a monolayer of xenon surface coverage can be expected.

The rate of buildup of xenon on a cold surface can be computed by evaluating the xenon arrival rate (as a result of xenon diffusion from the plasma generator) and loss rate (as a result of xenon evaporation at 100K from the cold optical surface).

The flux of neutral xenon arriving on an exposed surface is

$$f_{\text{arriving}} = n_0 \langle v_0 \rangle / 4,$$

where $n_0 = 10^{11}/\text{m}^3$ is the assumed neutral-xenon density, and $\langle v_0 \rangle = 194 \text{ m/s}$ is the mean xenon-atom velocity (assuming a 300K temperature). These approximate numbers give an arriving flux of about

$$f_{\text{arriving}} = 5 \times 10^{15} / \text{m}^2 \text{s}.$$

The loss flux can be estimated by assuming that there is a thin xenon-vapor layer above the cold surface that is in equilibrium with the adsorbed xenon immediately below it. This layer will have a pressure equal to the vapor pressure of xenon at 100K (i.e., 100 Pa). This pressure corresponds to a gas density near the surface of

$$n_s = P/kT_s = 10^{23} / \text{m}^3,$$

giving a flux of leaving xenon atoms of

$$f_{\text{leaving}} = n_s \langle v_s \rangle / 4 = 3 \times 10^{24} / \text{m}^2 \text{s}.$$

These simple calculations predict that if there were a surface layer of adsorbed xenon, it would desorb approximately 10^9 times faster than it could be replenished from ambient xenon. This calculation confirms what intuition suggests: unless the pressure of xenon gas that reaches cryogenic surfaces exceeds the 100-Pa vapor pressure of xenon at 100K, no frozen-xenon buildup will occur. Xenon pressures this high exist only inside the plasma generator itself, and only for a few seconds during gas-burst ignition.

While the foregoing calculations show that no macroscopic xenon-ice buildup can be expected, a small fraction of a monolayer of xenon will form on exposed surfaces, because arriving atoms spend a finite time on the surface before they are evaporated off. The equilibrium surface coverage increases with incident xenon flux, decreases with temperature, and varies somewhat with the composition of the optical surface. In a typical result,³ investigators found 0.08 monolayers of xenon on a palladium substrate at 100K; however, their incident xenon-atom flux was $f_{\text{arriving}} = 3 \times 10^{17} / \text{m}^2 \text{s}$, which is greater than our expected flux by a factor of ~ 40 . Very sophisticated experiments are required to detect even one monolayer; therefore, the buildup of xenon from the plasma generator should not affect the operation of any optical surfaces or sensors.

This Page Intentionally Left Blank

SECTION 8

SYSTEM CONSIDERATIONS

The exact vehicle and/or satellite on which the FMDS would be flown was not known at the time it was designed. Therefore, it was designed for what we considered to be standard and reasonable power, command, telemetry, and mechanical interfaces. The possibility now exists that the FMDS will be flown on the GOES IJK/LM series of spacecraft being built by Ford Aerospace & Communications Corporation. In this event, several changes to the FMDS are required, and the major ones are briefly described below.

- The resistors in the command interface need to be changed to accept 26-V signals instead of 5-V signals.
- An additional printed circuit card and/or interface box needs to be added to make the FMDS telemetry compatible.
- The power electronics must be compatible with a 29 to 43 Vdc input bus, instead of 28 ± 4 Vdc.
- Circuitry must be added to provide command ON/OFF of the housekeeping inverter, rather than being turned ON/OFF by the input power bus.
- The power MOSFETS in the inverters must be changed to the rad-hard version because of the seven-year life of the satellite (compared with a design for three-year life) and the fact that FMDS will be continuously connected to the bus for the full seven years.
- The plasma generator must be canted to point through the spacecraft center of gravity.
- The thrust axis of the plasma generator must be determined to within $\pm 0.25^\circ$.
- A mounting bracket must be provided to mount the FMDS under the honeycomb skin of the spacecraft, rather than on its outside surface.
- The thermal model must be modified to account for the new mounting configuration.

This Page Intentionally Left Blank

SECTION 9

CONCLUSIONS

The Flight Model Discharge System (FMDS) Program has completed its fourth year with no technical problems that will preclude its successful completion. The first flight ESA has been successfully built, tested, and delivered by the subcontractor. The remaining hardware for the first FMDS is nearing completion and is undergoing board and box level testing. System functional and environmental testing has not been started. Finally, the FMDS is being seriously considered to fly as an experiment on the GOES IJK/LM series of spacecraft.

This Page Intentionally Left Blank

BIBLIOGRAPHY

1. R.R. Robson, W.S. Williamson, and J. Santoru, "Flight model discharge system scientific report no. 2," AFGL-TR-86-0036, February 1986. ADA169423
2. J.C. Sturman, "Development and design of three monitoring instruments for spacecraft charging," NASA Technical Paper 1800, 1981.
3. E.R. Moog and M.B. Webb, "Xenon and krypton adsorption on palladium (100)," Surf. Sci. 148, 338-370 (1984).
4. R.R. Robson and W.S. Williamson, "Flight model discharge system scientific report no. 1," AFGL-TR-85-0044, March 1985. ADA160434
5. R.R. Robson, W.S. Williamson, and J. Santoru, "Flight model discharge system scientific report no. 3," AFGL-TR-87-0143, April 1987. ADA185657
6. S.L. Spiegel and H.A. Cohen, "Real time, automatic vehicle potential determination from ESA measurements, Part 2: The distribution function algorithm," AFGL-TR-85-0103(II). ADA162072
7. R.C. Olsen, "A threshold effect for spacecraft charging," J. Geophys. Res. 88, No. A1, 493-499 (January 1, 1983).
8. B.M. Shuman and H.A. Cohen, "Automatic charge control system for satellites," Proc. Spacecraft Environmental Interactions Technology 1983; AFGL-TR-85-0018, 1985.
9. B.M. Shuman, H.A. Cohen, J. Hyman, R.R. Robson, J. Santoru, and W.S. Williamson, "Automatic charge control system for geosynchronous satellites," Proc. Aerospace Environment at High altitudes and its Implications for Spacecraft Charging and Communications, AGARD conference proceedings no. 406, AGARD-CP-406, May 1987.

Unclassified

SECURITY CLASSIFICATION OF THIS PAGE

REPORT DOCUMENTATION PAGE				Form Approved OMB No. 0704-0188	
1a. REPORT SECURITY CLASSIFICATION Unclassified			1b. RESTRICTIVE MARKINGS		
2a. SECURITY CLASSIFICATION AUTHORITY			3. DISTRIBUTION/AVAILABILITY OF REPORT Approved for public release; distribution unlimited		
2b. DECLASSIFICATION/DOWNGRADING SCHEDULE					
4. PERFORMING ORGANIZATION REPORT NUMBER(S) HAC REF F4890			5. MONITORING ORGANIZATION REPORT NUMBER(S) AFGL-TR-88-0150		
6a. NAME OF PERFORMING ORGANIZATION Hughes Research Laboratories		6b. OFFICE SYMBOL (if applicable) HRL	7a. NAME OF MONITORING ORGANIZATION Air Force Geophysics Laboratory		
6c. ADDRESS (City, State, and ZIP Code) 3011 Malibu Canyon Road Malibu, CA 90265			7b. ADDRESS (City, State, and ZIP Code) Hanscom AFB Massachusetts 01731		
8a. NAME OF FUNDING/SPONSORING ORGANIZATION Air Force Geophysics Lab.		8b. OFFICE SYMBOL (if applicable) AFGL/PHE	9. PROCUREMENT INSTRUMENT IDENTIFICATION NUMBER F19628-83-C-0143		
8c. ADDRESS (City, State, and ZIP Code) Hanscom AFB Massachusetts 01731			10. SOURCE OF FUNDING NUMBERS		
			PROGRAM ELEMENT NO. 63410F	PROJECT NO. 2823	TASK NO. 01
			WORK UNIT ACCESSION NO. AA		
11. TITLE (Include Security Classification) Flight Model Discharge System (U)					
12. PERSONAL AUTHOR(S) R.R. Robson and W.S. Williamson					
13a. TYPE OF REPORT Scientific Report 4		13b. TIME COVERED FROM 3/87 TO 4/88		14. DATE OF REPORT (Year, Month, Day) 1988, June	
15. PAGE COUNT 92					
16. SUPPLEMENTARY NOTATION					
17. COSATI CODES			18. SUBJECT TERMS (Continue on reverse if necessary and identify by block number)		
FIELD	GROUP	SUB-GROUP	Spacecraft charging; Charge control system (CCS)		
			Spacecraft automatic active discharge system,		
			Flight model discharge system (FMDS)		
19. ABSTRACT (Continue on reverse if necessary and identify by block number)					
<p>The Flight Model Discharge System (FMDS) Program has completed its fourth year. The FMDS is a spacecraft charge control system designed to overcome the problem of charge buildup on a space vehicle which occurs during periods of adverse space environmental conditions. An overview of the FMDS system is presented, followed by an in-depth treatment of the significant technical developments that have occurred during the past year. The major areas covered include the plasma generator and electrostatic analyzer testing. <i>Keywords.</i></p>					
20. DISTRIBUTION/AVAILABILITY OF ABSTRACT <input type="checkbox"/> UNCLASSIFIED/UNLIMITED <input checked="" type="checkbox"/> SAME AS RPT. <input type="checkbox"/> DTIC USERS			21. ABSTRACT SECURITY CLASSIFICATION Unclassified		
22a. NAME OF RESPONSIBLE INDIVIDUAL G. Kenneth Yates			22b. TELEPHONE (Include Area Code) (617) 377-3991		22c. OFFICE SYMBOL AFGL/PHE

DD Form 1473, JUN 86

Previous editions are obsolete.

SECURITY CLASSIFICATION OF THIS PAGE

Unclassified